Chapter

14 The Parallel Universe: Parallel Imaging and Novel Acquisition Techniques

14.1 Introduction

As Figure 14.1 shows, in order to halve the scan time, the gradient slew rate must be quadrupled. Producing higher and higher gradient slew rates presents significant engineering challenges. However, we will also see in Chapter 20 that rapidly switched fields can lead to peripheral nerve stimulation, so physiology rather than physics may ultimately limit scanner speed. So does this mean fast imaging development has ground to a standstill? Surprisingly not, as even this fundamental limitation can be overcome, (or rather, circumvented) by using parallel imaging and reconstruction techniques together with phased array technology for even faster scanning. It must be stressed that parallel imaging methods are not sequences, but entirely new ways of acquiring and reconstructing images. The two classic formulations of parallel imaging are SMASH and SENSE, working in k-space and image space respectively. This chapter will explain the various types of parallel imaging and other novel reconstruction and acquisition techniques, how they work, what advantages they provide and the image quality trade-offs involved.

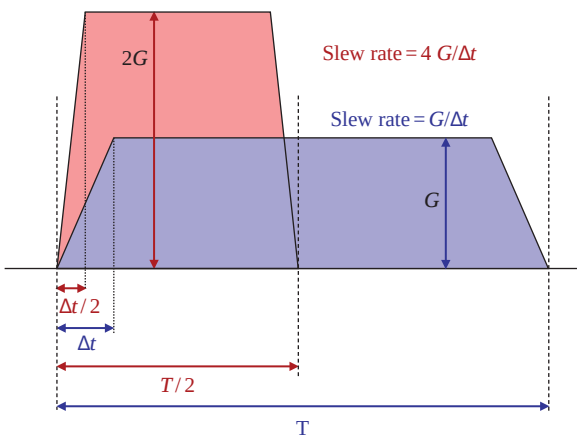

Figure 14.1 In order to halve the acquisition time while maintaining the same resolution and field of view, the gradient strength must be doubled and the gradient slew rate quadrupled.

In this chapter we will see that parallel imaging

- makes MR acquisitions faster by a factor known as the reduction factor *R*, by reducing the number of phase-encode steps you need to actually acquire an image;
- can be applied to any existing MR sequence, including EPI;
- is enabled by phased array technology and may be performed in k-space or in image space;
- involves an image quality trade-off.

Additionally

- non-Cartesian acquisition methods can offer some advantages such as very short echo times, self-navigation and increased SNR;
- compressed sensing is the next speed-up revolution in MRI;
- you will also learn lots of lovely new acronyms!

14.2 Groundwork

To understand parallel imaging we need to revisit two concepts considered earlier in the book, namely: array coils (Chapter 10) and phase encoding (Chapter 8). If you are confident you understand both of these you can skip forward to Section 14.2.3.

14.2.1 Simple Conceptual Explanation of k-Space and Phase Encoding

Phase encoding was explained in detail in Chapter 8. For the present purpose we need to see that each phase-encode gradient step adds a further 2π of phase change across the image field of view (Figure 14.2). Alternatively, we can say that each line of k-space is separated by 2π/FOV. Each phase-encoding step sensitizes the MR acquisition to specific patterns of signal distribution, or in other words, picks out a particular

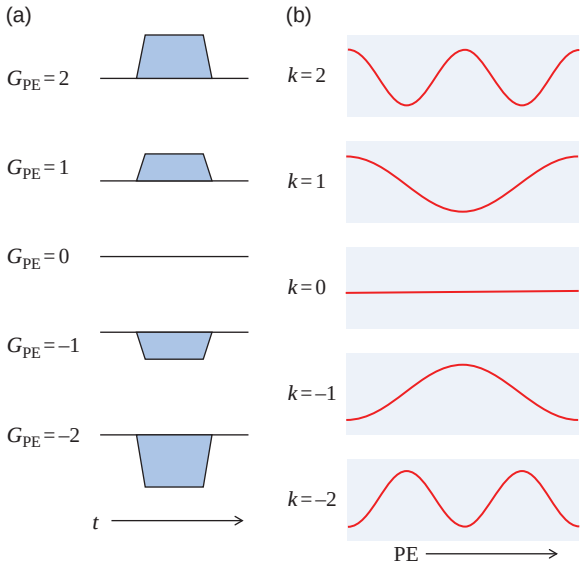

Figure 14.2 The effect of phase encoding on a uniform region of signal-producing material: (**a**) phase-encode gradient waveforms, (**b**) signal phase variation across the field of view.

spatial frequency of the image. The steps of phase encoding and signal acquisition need to be repeated until k-space is filled, prior to Fourier transformation to generate the final image. If we double the separation between the lines of k-space by skipping lines of k-space we halve the image field of view and if the imaged object exceeds this, aliasing or foldover will occur.

14.2.2 Basic Principles of Phased Arrays

The conventional use of phased array coils is to achieve superior SNR. Each array element is sensitive to a smaller volume of tissue than an equivalent larger coil. Inductively coupled noise, which usually dominates the noise formation process, has a theoretical strong dependence on the volume of tissue to which the coil is sensitive. The smaller array elements thus 'see' less noise than larger coils (Figure 14.3). Each array element has a separate receiver channel, with up to 32 channels being common. Additionally, arrays benefit from the combination of uncorrelated noise sources offering the same sort of advantage that quadrature coils have over linear coils (see Section 10.4.3). Separate reconstructions are carried out for each array element, with the final image being a combination of these. The increased SNR can be used to

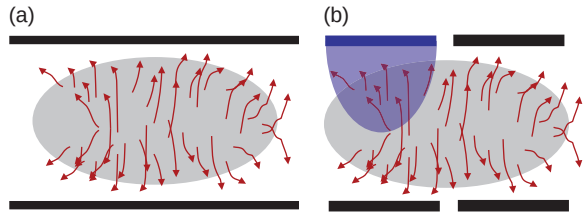

Figure 14.3 The inductive noise-reduction principle of phased array coils. (**a**) A larger single coil 'sees' more noise from the greater volume of tissue it surrounds. (**b**) Smaller coil elements are less sensitive to inductive noise while adequate signal coverage is achieved by combining images from the separate elements.

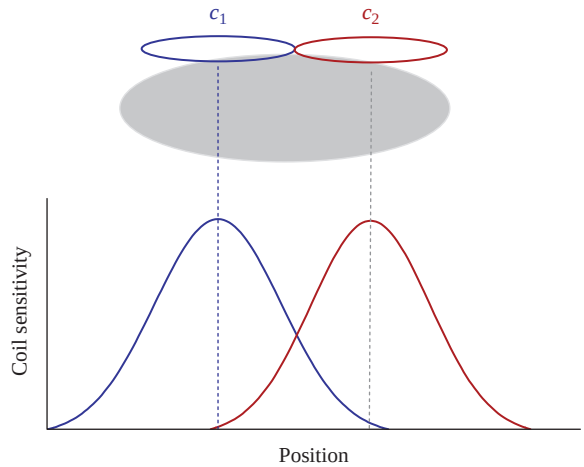

Figure 14.4 Coil sensitivity profiles: two loop surface coils.

achieve higher resolution, shorter scan times, greater anatomical coverage or a combination of all three. Many clinical applications would be impossible without array coils. In parallel imaging we are going to trade part of the superior SNR to give us shorter acquisition times.

14.2.3 Coil Sensitivity Profiles

In the conventional use of phased arrays, the images produced from each element are combined to form the resultant image. The spatial variations inherent to the individual coil responses, or the coil sensitivities, have been combined. This is illustrated in Figure 14.4, where individual sensitivity profiles are shown for two coils. The determination of array element sensitivity profiles or maps and the linear combination of signals from array elements are both crucial aspects of parallel imaging.

14.3 Making SENSE: Parallel Imaging in Image Space

In parallel imaging we are going to speed up scanning by acquiring fewer lines of k-space and using our knowledge of the array coils used to unravel the aliased images or to generate the missing lines of k-space. The former technique employs parallel imaging reconstruction in image space, the latter in k-space. In both methods the scan time is reduced by a reduction factor R:

$$\text{Scan time}_{2D} = \frac{\text{NSA} \times \text{TR} \times N_{PE}}{R \times \text{ETL}}$$

where N_{PE} is the full (unreduced) PE matrix size and ETL the echo train length or turbo factor (where appropriate) for 2D scans. For 3D scans

$$\text{Scan time}_{3D} = \frac{\text{NSA} \times \text{TR} \times N_{PE} \times N_{SS}}{R_{PE} \times R_{SS} \times \text{ETL}}$$

where R_{PE} and R_{SS} are reduction factors for each phase-encode direction.

14.3.1 SENSE

SENSE (**SENS**itivity **E**ncoding) was the first parallel imaging technique to be realized commercially (by Philips). ASSET on GE Healthcare scanners and SPEEDER (Toshiba) are broadly similar. In SENSE, a reduced k-space is acquired by using fewer phase-encode gradient steps in conjunction with phased array coil acquisition. A mathematical description is given in Box 'Making SENSE with Maths'.

SENSE reconstruction works post-Fourier transformation on the images. In a conventional acquisition if we omit every second phase-encode step we will halve the scan time, but will get an aliased image. In parts of the image aliased signal is superimposed upon unaliased signal. However, the position in the resultant image of the aliased signal contribution is entirely predictable from knowledge of the field of view. What is unknown is the intensity of the aliased component. The trick in SENSE is to apply knowledge of the sensitivities of the coil elements to calculate the aliased signal component at each point.

An example with a reduction factor of 2 and two coil elements is shown in Figure 14.5, where the point P in the aliased image can be seen to be composed of signal originating from two different locations: $S(y)$ from the true location y and $S(y + \Delta Y)$ from the aliased position. Provided we know the coil sensitivities we can calculate the true and the displaced signal components. Having computed the aliased signal component $S(y + \Delta Y)$, it can be reassigned to its proper location.

Figure 14.6 illustrates the acquisition and reconstruction with clinical images. First, sensitivity maps are generated for each coil element from a short, low-resolution calibration scan, then an aliased image is reconstructed for each element before being fed into the SENSE reconstructor to produce the final image.

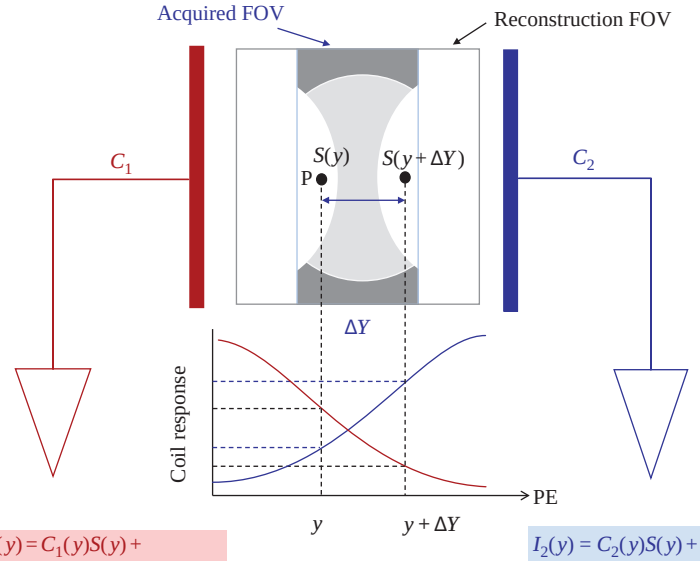

Figure 14.5 Image reconstruction in SENSE. Prior knowledge of the coil sensitivity profiles permits the unfolding of the image.

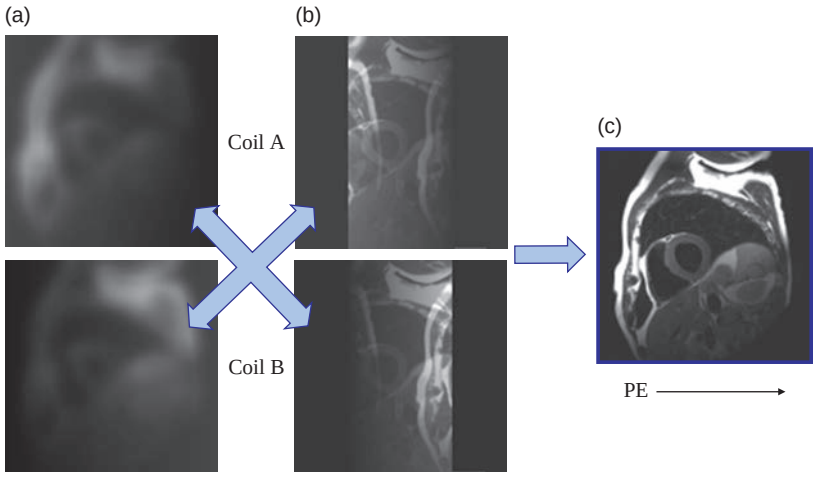

Figure 14.6 Example of SENSE reconstruction steps: (**a**) reference scans, (**b**) folded images from each element, (**c**) reconstructed SENSE image.

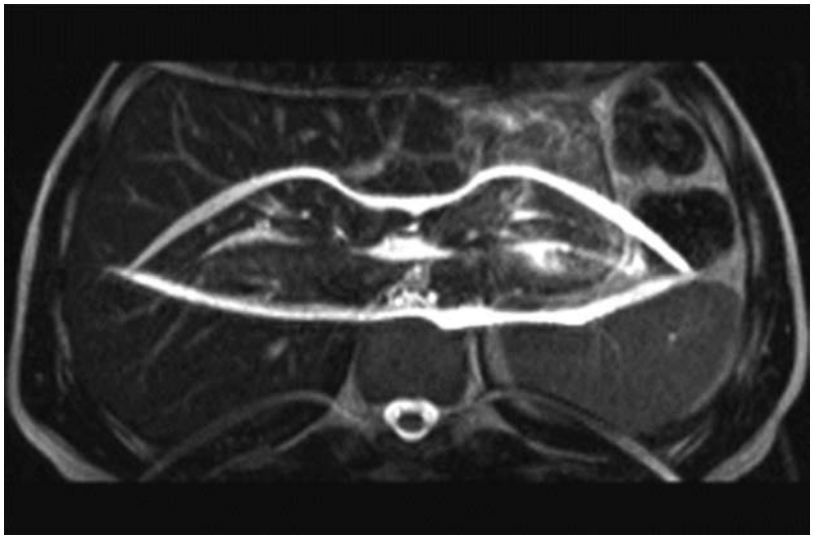

Figure 14.7 SENSE reconstruction 'hot lips' artefact resulting from attempting to use SENSE when the unfolded field of view does not contain all of the anatomical region of interest.

The principle can be applied for a higher reduction factor R as shown in Box 'Making SENSE with Maths'. For SENSE to work at all, there must be a coil sensitivity variation along the phase-encode direction. For array coils with appropriate geometry and in 3D FT acquisitions SENSE can be applied in both phase-encode directions, thereby increasing the overall reduction factor.

Another feature of SENSE is that the reduction factor can be any value between 1 and the number of coil elements. It is not restricted to integer values. In prescribing a SENSE scan the operator chooses the reconstructed FOV. This must encompass all the signal-producing material, otherwise serious artefacts will occur (Figure 14.7). In other words, SENSE cannot tolerate any inherent aliasing. The calibration procedure is explained further in Box 'To Auto-Calibrate or Not'.

Making SENSE with Maths

In the two-coil example of Figure 14.5, the signal at point y is made up of the correct signal for this position and one aliased signal. We can write

$$I_1(y) = C_1(y)S(y) + C_1(y + \Delta Y)S(y + \Delta Y)$$
$$I_2(y) = C_2(y)S(y) + C_2(y + \Delta Y)S(y + \Delta Y)$$

where I_1 and I_2 are the image intensities measured for each coil which have sensitivities C_1 and C_2. Hence we have two simultaneous equations and

two unknowns which can be solved exactly by algebra. The aliasing distance ΔY is

$$\Delta Y = \frac{\text{FOV}_{\text{rec}}}{R}$$

where FOV_{rec} is the reconstruction field of view for PE and R is the SENSE reduction factor. With higher R, we may have two or more aliased signals at point y as well as the correct signal, and we can write

$$\begin{aligned} t\,I_1(y) &= C_1(y)S(y) + C_1(y+\Delta Y)S(y+\Delta Y) \\ &\quad + \cdots + C_1(y+n_A\Delta Y)S(y+n_A\Delta Y) \\ I_2(y) &= C_2(y)S(y) + C_2(y+\Delta Y)S(y+\Delta Y) \\ &\quad + \cdots + C_2(y+n_A\Delta Y)S(y+n_A\Delta Y) \end{aligned}$$

where n_A is the number of aliased signals which is spatially variant and depends on the size of the object being imaged. If the object exactly fills the reconstructed FOV, then $n_A = R$ at all points; in all other cases $n_A \leq R$. We can formalize this in terms of image intensities $I_j(x,y)$ for each of j coil elements:

$$I_j(x,y) = \sum_{n=0}^{n_A} C_j(x, y+n\Delta Y)S(x, y+n\Delta Y)$$

If there are L coil elements, we can write L simultaneous equations as above, most conveniently represented in a matrix equation as

$$\begin{bmatrix} I_1(x,y) \\ I_2(x,y) \\ \vdots \\ I_L(x,y) \end{bmatrix} = \begin{bmatrix} C_1(x,y) & C_1(x,y+\Delta Y) & \cdots & C_1(x,y+n_A\Delta Y) \\ C_2(x,y) & C_2(x,y+\Delta Y) & \cdots & C_2(x,y+n_A\Delta Y) \\ \vdots & \vdots & \ddots & \vdots \\ C_L(x,y) & C_L(x,y+\Delta Y) & \cdots & C_L(x,y+n_A\Delta Y) \end{bmatrix} \cdot \begin{bmatrix} S(x,y) \\ S(x,y+\Delta Y) \\ \vdots \\ S(x,y+n_A\Delta Y) \end{bmatrix}$$

which is more economically expressed as

$$\mathbf{I} = \mathbf{CS}$$

and the solution arises from inverting the $L \times n_A$ element matrix C to obtain the true image signal $S(x,y)$ for every pixel. This is always possible if there are at least as many coil elements as the maximum number of aliased signals and if the coil sensitivities are sufficiently unique. Notice that since $R > n_A$ for the majority of images, it is possible for R to be greater than the number of elements in the coil. Prescan calibration data, or as in the case of mSENSE, reference lines, are required to obtain the coil sensitivities.

14.3.2 mSENSE

Modified **SENSE** (mSENSE) is a version of SENSE which does not require a separate calibration scan. Instead, additional lines are acquired at the centre of k-space during the diagnostic scan (Figure 14.8). These central lines are extracted for each coil element and used on their own to reconstruct low-resolution, unaliased images from each coil element which may then be used to provide sensitivity maps. A SENSE reconstruction algorithm can then be used to unfold the images from the sparse k-space data (the red arrows in Figure 14.8). The full-time saving by the reduction factor R is not achieved because of the additional lines required for calibration.

To Auto-Calibrate or Not

In the calibration method used by SENSE, low-resolution images are acquired from each array element and also from the body coil. The array element images are divided by the body coil image (to remove sensitivity variations due to anatomy rather than coil response). Then various image processing steps (thresholding, filtering, extrapolation, smoothing) are performed to produce the sensitivity map for each coil. Note that due to the thresholding step, the background noise is suppressed in SENSE images.

The calibration scan takes about 20 s and once acquired can be used on all subsequent parallel image acquisitions provided the geometry or the patient's position does not change. ASSET (GE) and SPEEDER (Toshiba) also require calibration scans. ASSET does not employ the body coil division step.

In mSENSE, GRAPPA and ARC (see Section 14.4.3) the calibration data are inherent to the main scan acquisition. No body coil image is required and there is no image division. This means that the background noise is not suppressed. Having the calibration (ACS) lines integral to the acquisition also means there will be no misregistration problem if the patient moves between scans. However, the scan time will be increased by the number of ACS lines used, thus the full reduction factor will not be realized. In GRAPPA, the ACS lines may also be included in the reconstruction, giving a slight increase in SNR.

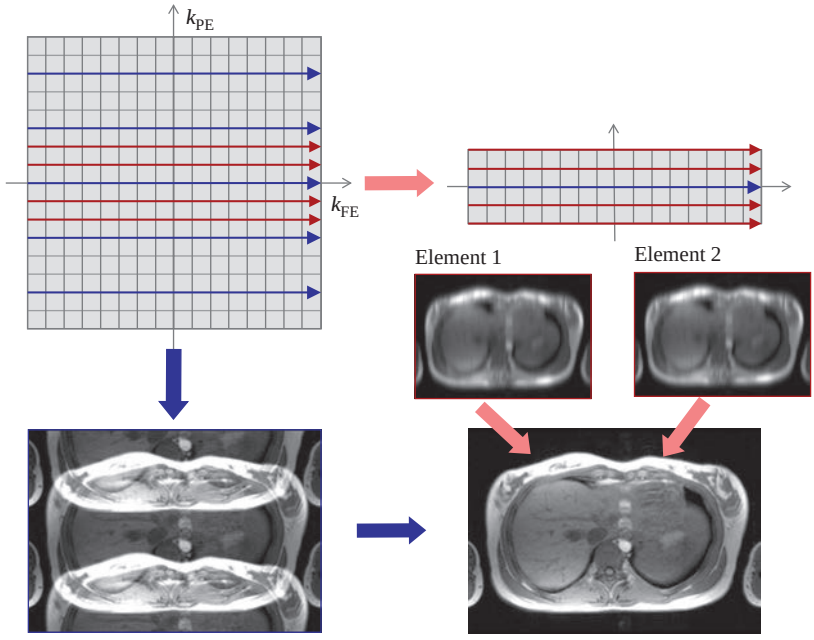

Figure 14.8 Modified SENSE (mSENSE). The centre of k-space is fully sampled and extracted for each coil to form a low-resolution image which can be used as a sensitivity map in a SENSE reconstruction. Images courtesy of Siemens Healthcare.

14.4 SMASH Hits: Parallel Imaging in k-Space

Historically SMASH (**SiM**ultaneous **A**cquisition of **S**patial **H**armonics) was the first parallel imaging technique. The term spatial harmonics refers to the spatial frequencies: SMASH works in k-space. It uses combinations of array coil element sensitivities to create virtual phase encoding. In principle it can be applied to any sequence. Just like SENSE, it reduces the number of phase-encode gradient steps you need, giving a scan time reduction by factor *R*.

14.4.1 SMASH

Looking back at Figure 14.2 we see the signal distributions in the phase-encode direction for various values of *k*. The principle of SMASH is simply to generate a similar pseudo k-space phase encoding by using the spatial response of the RF reception. In practice this means using arrays of coils and combining the various elements to obtain the required sinusoidal variations in response across space.

Figure 14.9 shows how two simple linear coils could be combined to produce either a uniform response by adding the signals together, or a non-uniform response which resembles a sinusoidal variation by subtraction of the coil sensitivities. In other words, by the appropriate combination of signals from different coil elements we can obtain a spatial signal distribution which can be made to match either zero spatial frequency (uniform response, $k = 0$) or the lowest non-zero spatial frequency ($k = 1$). In practice weighted combinations of the coil sensitivities are used. Figure 14.10 shows the coil weights necessary to produce k = 0 and k = 2 spatial harmonics for a notional eight-element array coil. Further details are given in Box 'More about spatial harmonics'.

This use of RF reception properties to achieve spatial encoding opens the intriguing prospect of an MR acquisition without the use of any phase-encode gradients. The RF engineering required to produce a sufficiently complex phased array coil is just too demanding at the moment – the coil would need at least 128 elements spread out along the phase-encode direction! Consequently, in SMASH a combination of phase encoding with gradients, and virtual phase encoding (with array coils) is applied. This is illustrated in Figure 14.11, showing the phase change over the FOV for the $k = 2$ PE gradient from the uniform coil combination ($\Delta k = 0$). By combining the coils differently a modified response ($\Delta k = 1$) is obtained and when added to the effect of the gradient produces a line of virtual phase encoding with $k = 3$. Figure 14.12 shows combinations of gradient and array coil phase encoding to generate six lines of k-space from only three actual acquisitions. In this

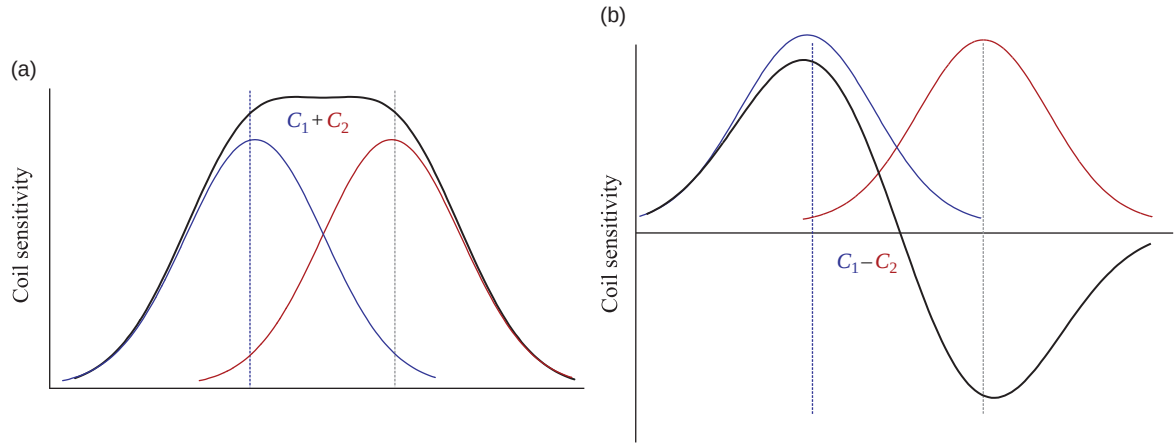

Figure 14.9 Coil sensitivity profile combinations for two loop surface coils: (**a**) coil combination (addition) to achieve uniform spatial response, (**b**) coil combination (subtraction) to produce non-uniform spatial response.

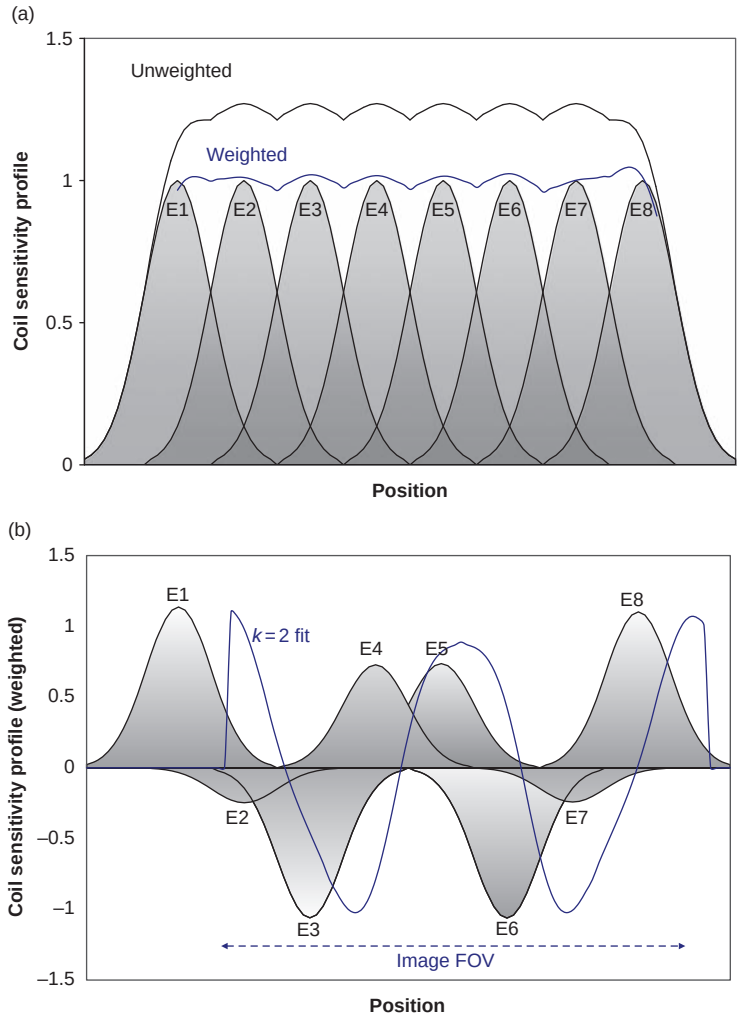

Figure 14.10 (**a**) Unweighted and optimally weighted coil combinations to produce a uniform (k = 0) response for an eight-element array coil. (**b**) Weighted coil sensitivity functions to produce the second harmonic (k = 2). Shaded areas represent the coil sensitivity profiles multiplied by their respective weight.

example, then, we can halve the number of phase-encode gradient steps required, and therefore halve the number of excitations required and halve the scan time. The reduction factor R is therefore equal to 2.

The acquisition in k-space is illustrated in Figure 14.13a, where we see that k-space is filled completely using a sparser set of phase-encode gradient steps (represented by the blue arrows) and the synthesizing of virtual phase-encode lines (the dotted lines) from the combinations of the coils.

More About Spatial Harmonics

The purpose of phase encoding is to produce a linearly varying phase change to the MR signal along the phase-encode axis, as illustrated in the clockface diagram in Figure 14.11. In order to generate the rotational nature of phase encoding, we need to add sine and cosine functions (see appendices A.2 and A.5). Mathematically this is:

$$\exp(i2\pi y k_{PE}) = \cos(2\pi y k_{PE}) + i\sin(2\pi y k_{PE})$$

remembering that k-space uses complex maths. The first harmonics are shown in Figure 14.14 for the example of an eight-element coil, along with the $\Delta k = 1$ combination. The figure shows both the calculated harmonics and the ideal ones.

Figure 14.14 also shows the higher harmonic, $\Delta k = 3$, for the same eight-element coil, showing that significant deviations exist between the ideal and the fitted harmonics. Errors in the generation of the coefficients will result in image artefacts (see Figure 14.19).

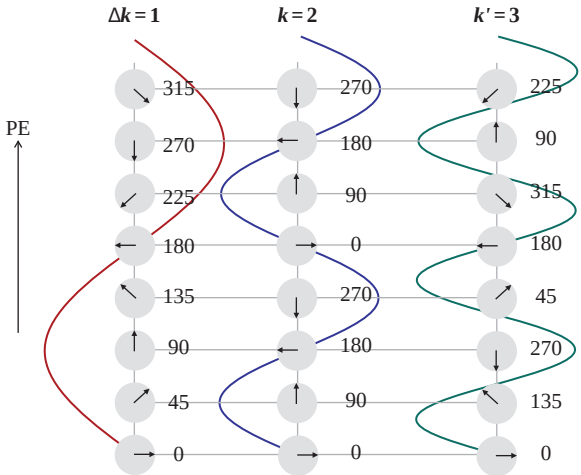

Figure 14.11 Virtual phase encoding from combinations of coil sensitivities ($\Delta k = 1$) combined with an actual phase encoding line ($k = 2$) produces an additional line of phase-encoded signal $k' = 3$.

14.4.2 Auto-Calibrating SMASH

The constraints of coil design make true SMASH very hard to realize on a clinical scanner. In order to make SMASH techniques more applicable to real phased array coils a change of strategy was needed. Instead of making coils to give a 'spatial frequency-type' signal response, why not accept whatever spatial sensitivity response the coils actually give and then work out how to combine their signals to get the desired lines of k-space? The first technique to do this was Auto-SMASH. The principle is shown in Figure 14.13b, where a reduced k-space is acquired by skipping lines (e.g. every third line to give a reduction factor $R = 3$). However, we also acquire additional 'auto-calibrating signal' (ACS) lines near the centre of k-space. The scanner then

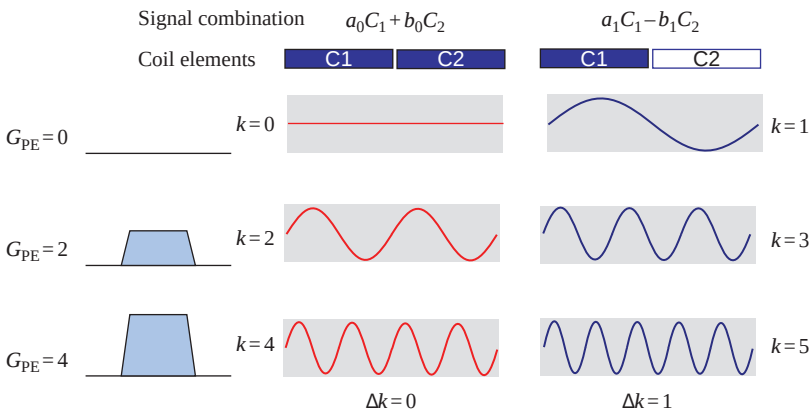

Figure 14.12 The addition of gradient phase-encoding and RF coil combinations produces additional virtual lines of k-space. In this example two lines of k-space can be acquired per gradient, the original with $\Delta k = 0$ and one additional with $\Delta k = 1$.

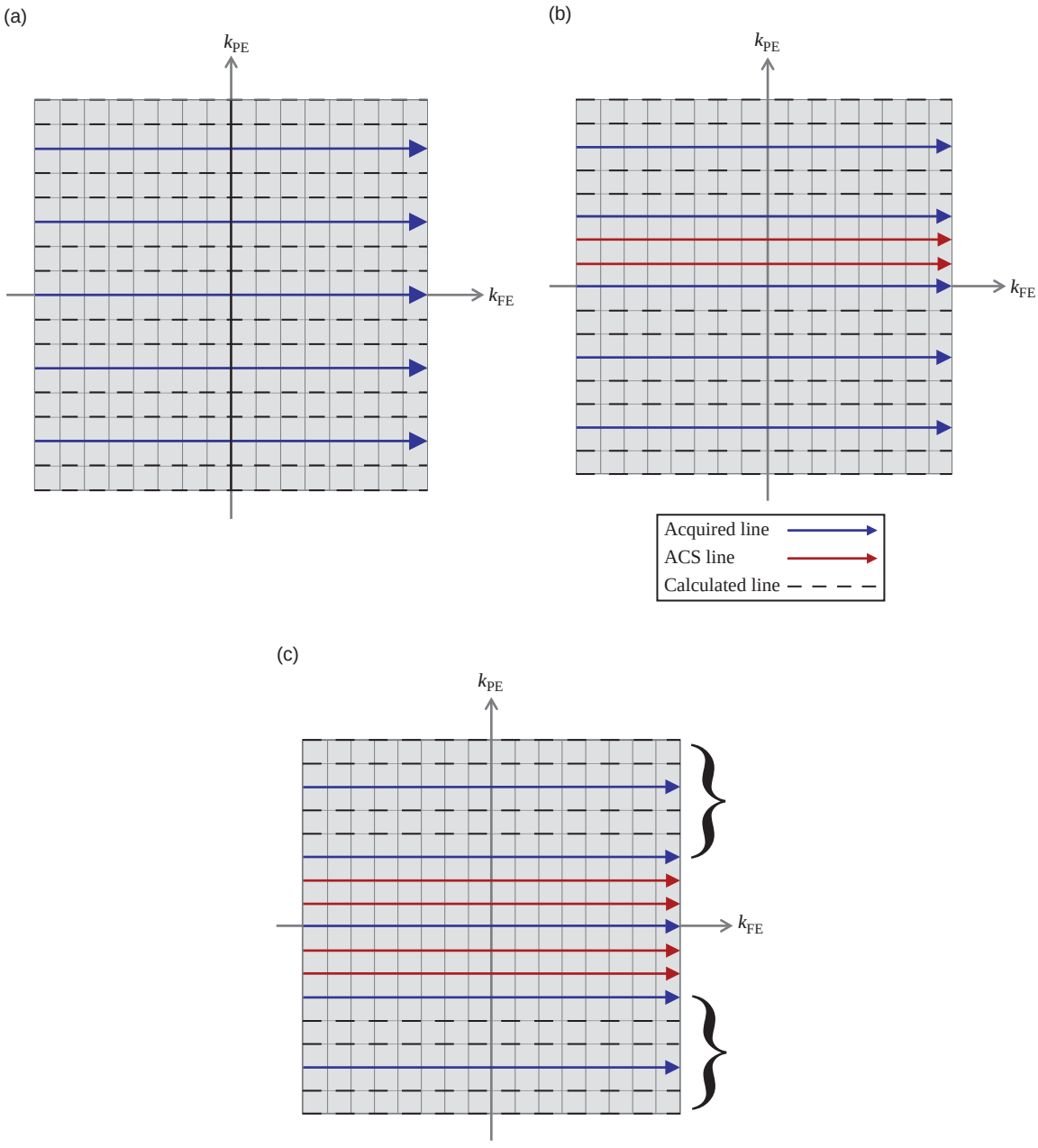

Figure 14.13 k-space scheme for (**a**) SMASH, (**b**) Auto-SMASH with two ACS lines and (c) VD-Auto-SMASH where an outer reduction factor (ORF) applies away from the centre of k-space. In each example $R = 3$. Arrowed lines are acquired with gradients, the interspersed (non-arrowed) lines are computed from combinations of the coil element signals. The fully filled k-space is Fourier transformed to generate the image.

computes from the signals acquired from the array coil elements the nearest linear combination of these signals to match the actual acquired ACS line. The coefficients calculated can then be applied throughout the remainder of k-space to fill in the unacquired lines, before standard reconstruction by Fourier transformation. In practice a minimum of R-1 ACS lines are required.

Variable density Auto-SMASH (VD-Auto-SMASH) extends the above principle, but adds additional ACS lines, illustrated in Figure 14.13c. This makes it more robust from artefacts and

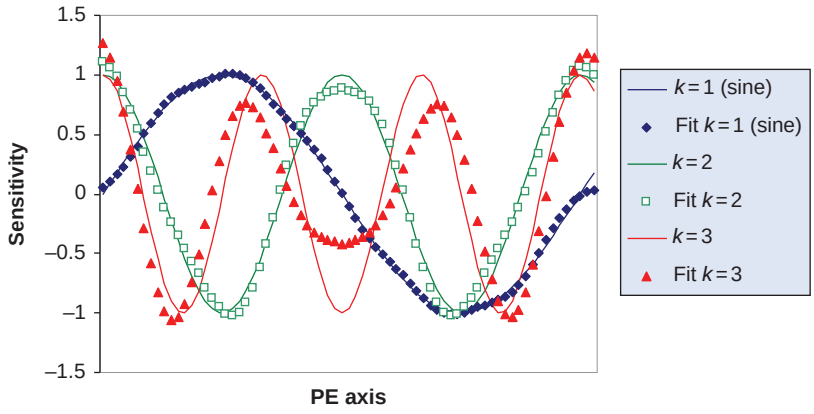

Figure 14.14 Fitted (calculated) and ideal sensitivity profiles for Δk = 1 (sine) and cosine profiles for Δk = 2 and 3. Solid lines show the ideal response, points show the weighted fits for an eight-element array.

reconstruction errors. The centre of k-space is more highly sampled and we can talk of an inner and an outer reduction factor. The scan time compared with Auto-SMASH will be longer because of the additional ACS lines. As in Auto-SMASH, a composite k-space (i.e. just one for all the array elements) is acquired and estimated.

SMASH and k-Space Methods

As usual in MRI, those of a mathematical nature get it easy as the whole thing can be reduced to one equation:

$$S(k_x, k_y) = \iint \rho(x, y) \cdot C(x, y) \cdot \exp\left(\frac{-t}{T_2^*}\right) \cdot \exp(i2\pi x k_{FE}) \cdot \exp(i2\pi y k_{PE}) \cdot dx dy$$

This is similar to the equation for 2D FT given way back in Chapter 7, but with one additional term: $C(x,y)$ which represents the coil sensitivities. For an array of coils with sensitivities $C_j(x,y)$

$$S(k_x, k_y) = \iint \rho(x, y) \cdot \left[\sum_j n_j C_j(x, y)\right] \cdot \exp\left(\frac{-t}{T_2^*}\right) \cdot \exp(i2\pi x k_{FE}) \cdot \exp(i2\pi y k_{PE}) \cdot dx dy = \sum_j n_j \cdot S_j(k_{FE}, k_{PE})$$

where n_j are weighting factors for a superposition of coil and signal sensitivities. By judicious choice of weights we can obtain the combinations

$$\sum_j n_j C_j(x, y) = 1 \quad \text{or} \quad \sum_j n'_j C_j(x, y) = \exp(i2\pi \cdot y \Delta k_{PE})$$

where Δk is a step in spatial frequency. Using the first of these yields the standard 2D FT equation for a uniform coil. Using the second gives

$$S' = \iint \rho(x, y) \cdot \exp\left(\frac{-t}{T_2^*}\right) \cdot \exp(i2\pi x k_{FE}) \cdot \exp(i2\pi y [k_{PE} + \Delta k_{PE}]) \cdot dx dy = S(k_{FE}, k_{PE} + \Delta k_{PE})$$

which is the acquired line of k-space offset by Δk. With the appropriate linear combination of coil signals we can therefore acquire purely gradient-phase-encoded signals or we can calculate additional virtual lines of k-space without having to acquire them.

In SMASH the sensitivities are computed from a calibration scan. In Auto-SMASH and GRAPPA additional auto-calibration signal (ACS) lines are acquired and the coil weights calculated from a fit of the ACS data with the known (acquired) neighbouring line or lines:

$$S(k_{FE}, k'_{PE}) = \sum_j n_j S_j(k_{FE}, k_{PE})$$

thus the coefficients n_j can be calculated to give a particular k-space offset. ARC extends this to three dimensions.

14.4.3 GRAPPA and ARC

GRAPPA (**Gene**ralized **A**uto-calibrating **P**artially **P**arallel **A**cquisitions) is a further extension of the Auto-SMASH principle. GRAPPA is illustrated in Figure 14.15. It deploys multiple ACS lines and uses data from every coil for the fitting of the appropriate weights for each ACS line. A separate sub-k-space

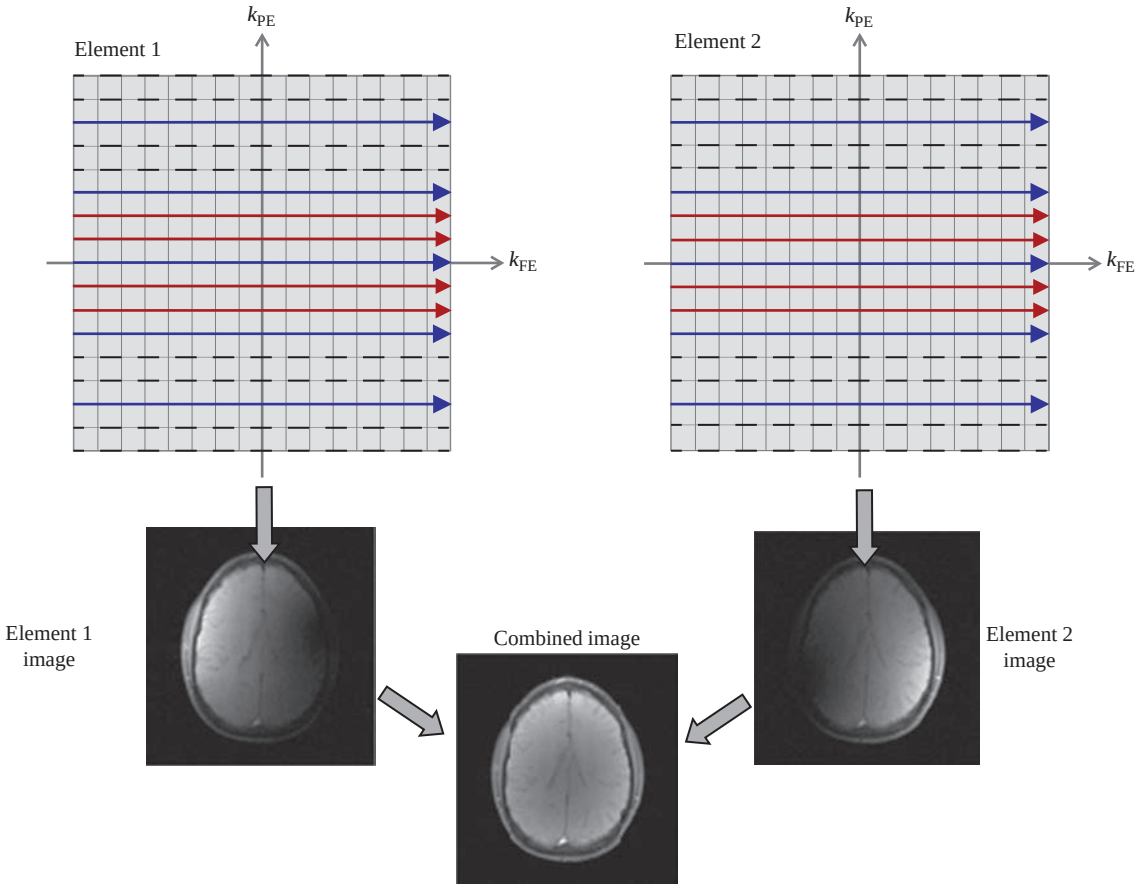

Figure 14.15 GRAPPA acquisition and reconstruction with $R = 2$. A separate k-space for each coil element is generated using multiple ACS lines and signal combinations from all the coil elements. Each element's k-space is Fourier transformed to generate images from each element which are then combined as in conventional phased array reconstruction.

is filled for each array element, which is then reconstructed, giving an image for each element. These separate images are then combined by the usual 'sum-of-squares' algorithm used in conventional array coil reconstructions. GRAPPA has been implemented commercially in Siemens scanners where the reduction factor is known as the iPAT factor and parallel imaging (both mSENSE and GRAPPA) goes under the generic name iPAT (where PAT stands for Parallel Acquisition Technique and the 'i' stands for 'integrated' – but we suspect is really just to appear trendy). ARC (Auto-calibrating Reconstruction for Cartesian imaging) is a 3D variant of this technique implemented on GE Healthcare scanners.

14.4.4 Air on a g-Factor: CAIPIRINHA

The principles of undersampling of k-space used in parallel imaging for 3D scans can be extended to more exotic acquisition patterns. For a given R factor, the g-factor (see Section 14.6) can be improved by increasing the distance between k-space points, particularly by introducing some asymmetry. In SENSE and GRAPPA and their equivalents we skip lines in both k_y and k_z, producing a regularly undersampled 3D k-space. Looking at Figure 14.16a we see a regularly undersampled k-space, looking at the k_y–k_z plane. However, other patterns are possible with the same undersampling factor, as shown in Figure 14.16b; we can characterize them by their diagonal shift Δ. As with simple ($\Delta = 0$) undersampled acquisitions, these patterns result in aliasing. However, the location of the aliasing can be better controlled and shifted to the edges of the FOV. This can result in a superior g-factor (see Figure 14.19), resulting in reduced artefacts, less dependence upon the coil array geometry and ultimately allowing the potential for higher acceleration

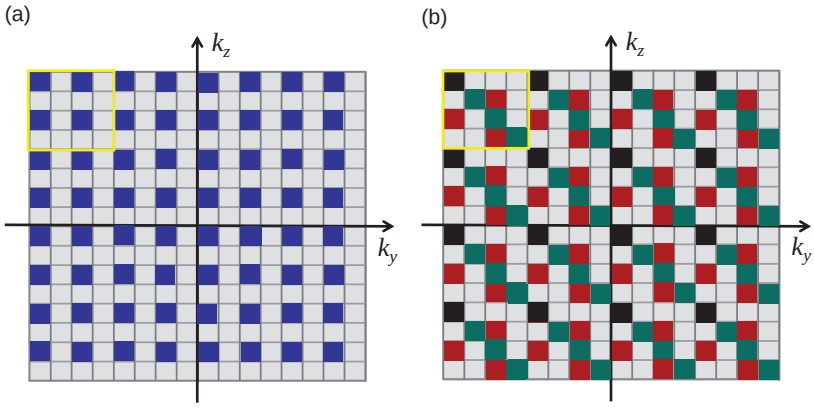

Figure 14.16 (**a**) Conventional parallel imaging k-space acquisition scheme in two PE directions with combined $R = 4$. (**b**) Two CAIPIRINHA k-space acquisition schemes, both with $R = 4$ and $\Delta = 1$, shown in green and red. The black points are acquired for both.

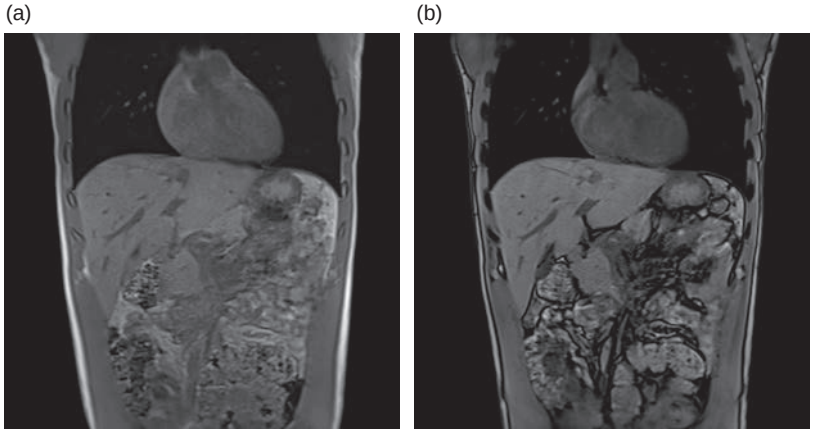

Figure 14.17 CAIPIRINHA images: (**a**) 3D-VIBE in-phase, (**b**) 3D-VIBE out-of-phase, reduction factor 2 × 3 = 6, 128 slices acquired in 20 s. Courtesy of Siemens Healthcare.

factors. This type of acquisition is commercially available on Siemens systems, under the name of CAIPIRINHA (**C**ontrolled **A**liasing **I**n **P**arallel **I**maging **R**esults **IN** **H**igher **A**cceleration). CAIPIRINHA uses a GRAPPA-style reconstruction, but SENSE can also be used (with the name 'diamond SENSE'). Figure 14.17 shows some representative CAIPIRINHA images.

14.5 Undersampling by Simultaneous Multi-Slice Excitation

Undersampling in the slice direction works easily for 3D acquisitions, but it is less obvious to see how to undersample a 2D multi-slice acquisition. We can't skip phase-encoding steps in the slice direction, because it isn't part of the pulse sequence. However, we can use so-called multi-band RF pulses to generate simultaneously excited slices, two or more at a time. Multi-band excitation has been around for a long time: it is used (on some systems) whenever you plan two parallel saturation bands (see Box 'Seeing Double: Exciting More than One Slice'), and for a few years in the early 1990s it was a feature on GE Healthcare systems, called **P**hase **O**ffset **M**ulti-**P**lanar (POMP). By modulating the phase of the RF excitation pulse, it is possible to produce slices with distinctly assigned phases, e.g. four slices can be excited at 0°, 90°, 180° and 270°. For (turbo) spin-echo scans, each of the 180 refocusing RF pulses also has to be phase-modulated.

Phase modulation of the different slices can be done in different ways. For example, in multi-slice GE imaging, phase modulation of the RF pulse can be used along with the cosine amplitude modulation. In EPI, a series of 'blip' gradients is added on the slice-select axis, coinciding with the normal phase-encode

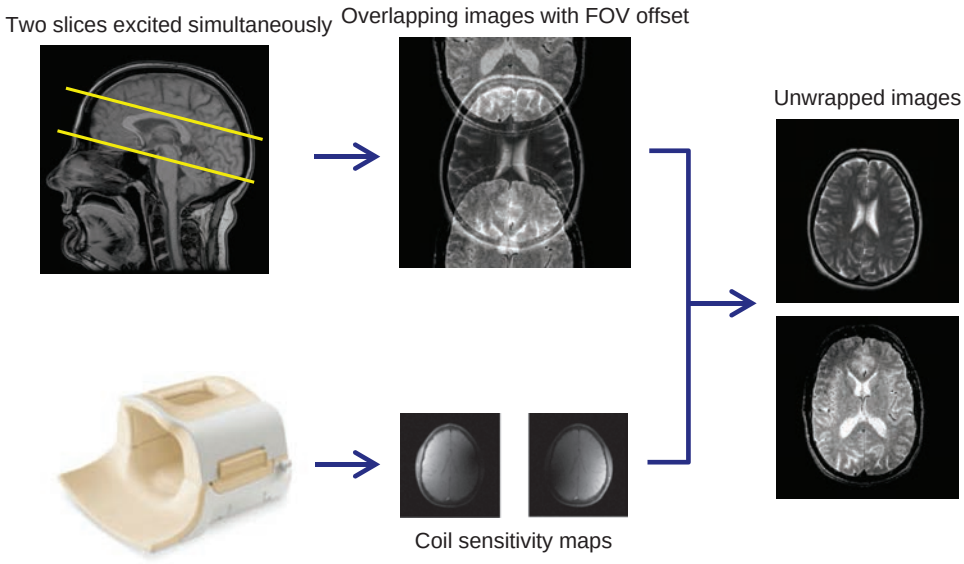

Figure 14.18 Principle of using controlled aliasing to separate simultaneously acquired slices.

blips. Fourier transformation of the signal from multi-band excitation in combination with phase-offsets will result in all the slices being aliased into a single image, with each slice offset in a controlled manner (by the Fourier transform shift theorem) within the field of view. If the coil sensitivities are known, it is possible to use a modified version of parallel reconstruction (i.e. the SENSE or GRAPPA algorithm) to separate the slices and generate the unaliased images (Figure 14.18). There must be sufficient separation of the receive coil elements along the slice direction, or separation of the excited slices, to preserve a low g-factor. At the time of writing, this technique is not commercially available, but it is known on Siemens systems as MS (**M**ulti-**S**lice) CAIPIRINHA (even though there's really no relationship to the other CAIPIRINHA) and on other systems as **M**ulti-**B**and (MB) SENSE.

In theory, simultaneous multi-slice excitation has no SNR disadvantage, unlike other parallel imaging methods. This is because the reduction factor R is compensated by the higher signal from N_{slices} being simultaneously excited (see Box 'SNR in Parallel Imaging'). However, in practice the g-factor will be slightly compromised by the geometry of the coil. Multi-band excitation can also be combined with in-plane GRAPPA or SENSE, provided the total g-factor is not increased too much.

Seeing Double: Exciting More than One Slice

Converting an excitation RF pulse to select two physical locations is achieved by multiplying it by a cosine function:

$$FT\{\cos(2\pi f_{sep}t)\} = \frac{\delta(f - f_{sep}) + \delta(f + f_{sep})}{2}$$

where f_{sep} is related to the required separation of the two slices, and δ represents a delta function. The frequency of the cosine can be calculated from the bandwidth of the RF pulse, and the gradients being used. This is also known as Hadamard excitation or double-sideband excitation. To preserve the original flip angle in the slices, it is necessary to double the peak B_1 and therefore double the SAR. For spatial sat bands, the advantage of multi-band excitation is that the time taken is halved.

14.6 Image Quality in Parallel Imaging

We saw in Chapter 6 that the image SNR was dependent upon the number of phase-encode lines acquired. This is also true in parallel imaging. So if we use a reduction factor R, then the SNR will be reduced theoretically by at least $\sqrt{R}$. In practice it will also be reduced by a geometric efficiency factor g, which is dependent upon the geometrical arrangement of the array elements and their sensitivities. Figure 14.19 shows the dramatic

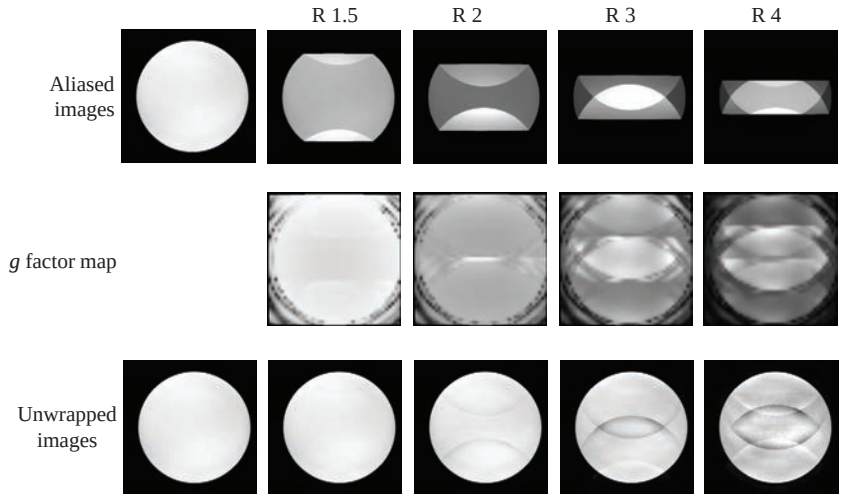

Figure 14.19 Image noise and reconstruction artefacts in SENSE at various reduction factors. Image courtesy of Philips Healthcare.

change of image quality with increasing R resulting from deterioration of the g-factor. Of course, the extent to which this occurs is dependent upon the number and arrangement of the array coil elements as well as the overall R-factor. More information is contained in Box 'SNR in Parallel Imaging'.

SNR in Parallel Imaging

The SNR in SENSE can be expressed as

$$\mathrm{SNR}_{\mathrm{SENSE}} = \frac{\mathrm{SNR}_{\mathrm{full}}}{g\sqrt{R}}$$

where g is a geometry factor which is always greater than or equal to 1, and is not spatially uniform across the image. An additional feature of SNR in SENSE is that the noise is not uniformly distributed across the image as in conventional acquisitions. This can be seen in Figure 14.19 for different R with the level of noise and artefact increasing with R.

The SNR in mSENSE and GRAPPA does not have such a simple relationship with R, as ACS lines can be used in the reconstruction to boost the SNR. Like SENSE, the noise varies spatially across the image in SMASH-type techniques.

In simultaneous multi-slice imaging, e.g. the so-called MS-CAIPIRINHA, the loss of SNR due to the reduction factor R is balanced by the number of simultaneously acquired slices:

$$\mathrm{SNR} = \sqrt{N_{\mathrm{slices}}}\frac{\mathrm{SNR}_{\mathrm{full}}}{g\sqrt{R}}$$

This means that the only SNR loss (compared to the regular multi-slice acquisition) is due to the g factor.

If too high a reduction factor is used then artefacts will appear in the image. These are shown for mSENSE and GRAPPA in Figure 14.20. Artefacts also appear if too few ACS lines are used in the auto-calibrating techniques. Typical parallel imaging artefacts are increased noise in the centre of the image (or wherever the coil sensitivities are weakest), and residual foldover ghosts, particularly if there is a very strong signal (like fat on T_1-weighted images).

We have already noted that for a SENSE acquisition, the field of view must be sufficiently large to encompass all the signal-producing regions. If it is not, then the images cannot be unfolded properly (Figure 14.7). However, SENSE can now be combined with no-phase-wrap in a flexible way which allows the user to achieve a scan time reduction overall.

In single-shot techniques like SS-TSE and EPI, parallel imaging can actually improve image quality by reducing T_2 blur and geometric distortion by shortening the echo trains (Figures 14.21 and 14.22). More details are given in Box 'Parallel EPI'.

Parallel EPI

Figure 14.23a shows that with parallel imaging the length of the echo train is reduced. The shorter echo train results in a higher PE bandwidth and hence less susceptibility distortion artefacts and reduces the minimum TE. Figure 14.23b shows the resulting k-space trajectory.

The single-shot nature of EPI, however, has implications for the reference images and calibration

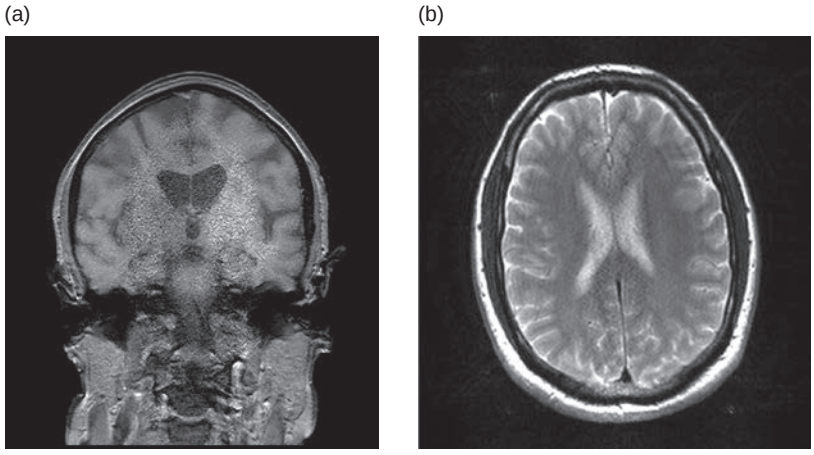

Figure 14.20 Parallel imaging artefacts from using too high a reduction factor: (**a**) SENSE, (**b**) GRAPPA.

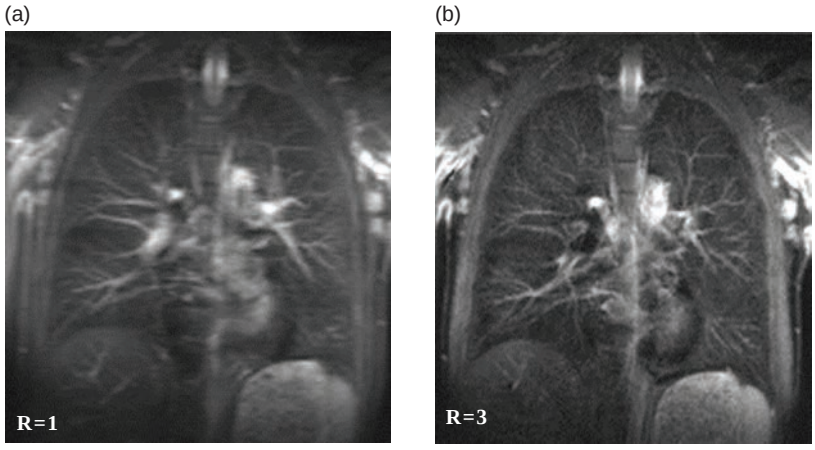

Figure 14.21 Reduction of T_2 blurring in HASTE imaging of the lungs. (**a**) Conventional 128 × 256 (207 ms), echo spacing 2.88 ms; (**b**) 256 × 256 (149 ms), effective echo spacing 0.96 ms. Images courtesy of Siemens Healthcare.

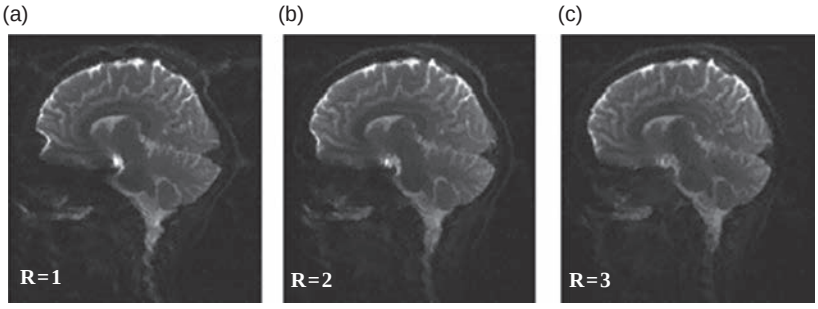

Figure 14.22 Parallel imaging reduces T_2^* distortion in EPI, by shortening the echo train length (increasing the PE bandwidth): (**a**) conventional, (**b**) $R = 2$, (**c**) $R = 3$. Images courtesy of Siemens Healthcare.

procedure. For SENSE and similar techniques, a standard calibration is run prior to the EPI acquisition(s), as for other sequences. For GRAPPA, the autocalibration traversal of the centre of k-space takes place before the reduced acquisition. In a repeated series of acquisitions as required for fMRI, this results in one additional 'TR' period. Another odd thing about EPI-GRAPPA is that, because the ACS data are real data and can be used in the reconstruction, the SNR for a reduction factor of 2 is higher than without parallel imaging, even if we control for the change of TE. For $R = 3$ and above SNR and image quality are degraded as the fitting to the ACS lines becomes more approximate.

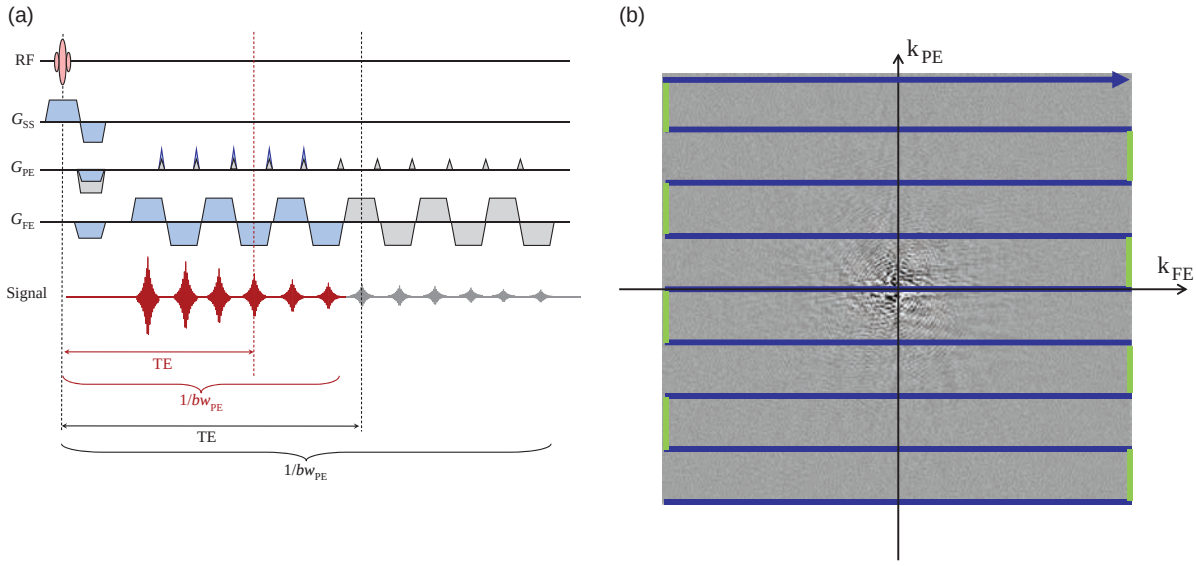

Figure 14.23 Parallel imaging and EPI. (**a**) EPI sequence corresponding to k-space in (a) with (blue) and without (blue) a reduction factor of 2. The use of parallel imaging reduces TE and increases the PE bandwidth, resulting in less susceptibility distortion. (**b**) k-space path of EPI with $R = 2$.

Clinical Benefits of Parallel Imaging

The benefits to parallel imaging can be summed up by the 'five Fs': faster, further, finer, (more) faithful and fainter (meaning quieter).

Figure 14.24 illustrates how shorter scan times can be achieved with very little discernible loss of image quality, but remember SNR is always reduced by at least $1/\sqrt{R}$, so use sparingly and only when you have to. Faster scanning also means shorter breath-holds with the potential for reduced respiratory motion artefact or the second 'F', further, or more slices per breath-hold. The application of even a modest reduction factor can enable successful breath-hold acquisition (Figure 14.25).

The reduction in the number of phase-encode steps acquired means that higher matrices, and hence better resolution, finer images, may be acquired within a reasonable scan time (but with a massively reduced SNR). Thus a 1024 matrix image using $R = 2$ can be acquired in the same time as a convention 512 matrix image (Figure 14.26).

Parallel imaging should be used whenever possible for echo planar acquisitions (EPI) to reduce the effect of susceptibility artefacts. It also enables a shortening of TE, very useful in DWI and DTI. For high-field systems, the susceptibility distortions in EPI can be particularly bad. Parallel imaging helps reduce this. Also, particularly for EPI, parallel imaging can help to reduce the acoustic noise.

There is an additional 'F' which is particularly relevant to high-field MR systems: fry. We don't want to overheat our patients! As the SAR increases with the square of field strength (or frequency), high-field systems (e.g. 3 T and above) are potentially limited by the permissible SAR. Of course these limits prevent us from frying our patients, but they do result in a need to lengthen TR, or reduce the number of slices or the echo train length. Parallel imaging helps by reducing the number of RF pulses required to form an image, and indeed, without it, even the simplest head scan can prove problematical at 3 T.

14.7 k-t BLAST

This technique is only available on some systems, but it is very promising for dynamic techniques such as cardiac imaging and dynamic contrast enhancement. k-t BLAST (**B**road-use **L**inear **A**cquisition **S**peed-up **T**echnique) takes advantage of the fact that most of the image does not change at all during these acquisitions. For example, in a typical short-axis cine of the heart, the chest wall, lungs, spine and muscles do not

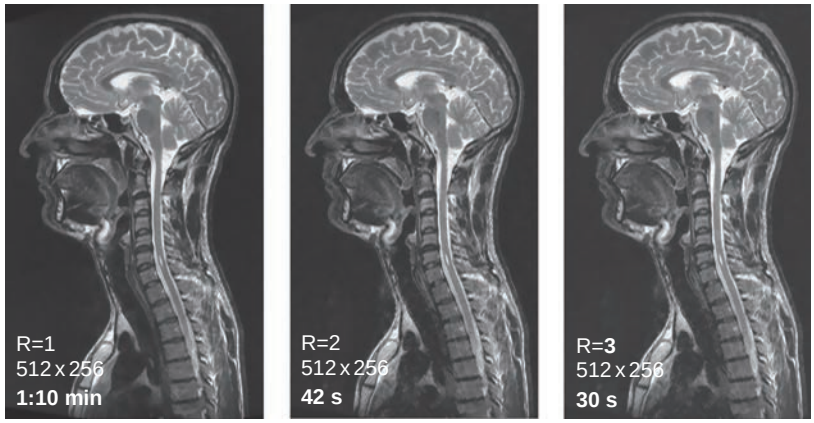

Figure 14.24 Use of parallel imaging (GRAPPA) to speed up T_2-weighted TSE scans. Images courtesy of Siemens Healthcare.

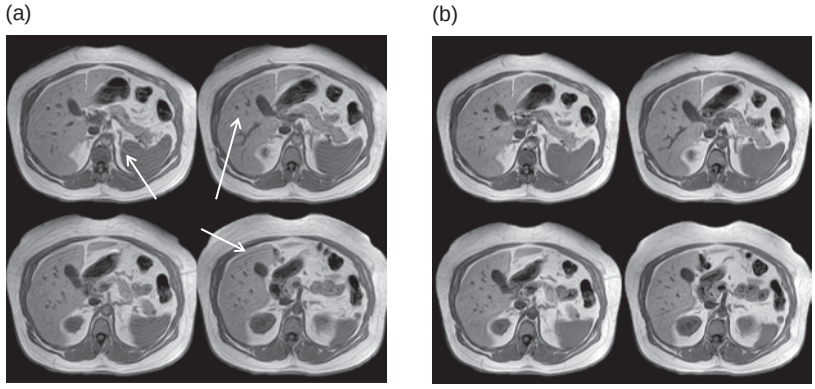

Figure 14.25 Use of SENSE to obtain better slice coverage within a breath-hold, resulting in reduced motion artefact (arrowed), (**a**) without SENSE, 22 s, (**b**) with SENSE, 13.5 s. Images courtesy of Philips Healthcare.

vary (much) from one frame to another. Once we have the first frame, these voxels do not need to be re-sampled during the rest of the cine. The remaining voxels can therefore be sampled quicker and provide better temporal and/or spatial resolution.

Figure 14.27 illustrates the principle for a single line through the cardiac frame. If we take the Fourier transform of this line through time, we find ourselves in x-f space, which shows the spectrum of motional frequencies. In the middle are all the voxels which do not change through the frames of the cine acquisition: out to the edges are the faster moving voxels which represent the ventricle walls and moving blood. It is obvious that most of this space is empty!

In normal imaging, every point in k-space is sampled at each of *t* time-points. By skipping some of the k-space points for some of the time-points, k-t space is undersampled. In x-f space, the periodic nature of the signal means they are folded in. Reconstruction of these signals will give foldover in real space and undersampling of the temporal frames, just like real-space signals are folded in during parallel imaging. To unfold the signal intensities, k-t BLAST uses a set of training data, usually a low-resolution cine with relatively few frames (Figure 14.28). The training data give an estimation of the signal distribution in x-f space. Combining the training data with the undersampled dynamic data allows the reconstructor to produce the final cine images.

k-t SENSE is k-t BLAST plus sensitivity encoding. By using the coil sensitivities of a multi-element receive coil, k-t space is undersampled even more, allowing speed-up factors up to 8. The reduced scan time can be traded for more slices (better coverage), higher spatial resolution, better temporal resolution or a combination of all three. For example, velocity mapping through the aorta can be achieved in a 10 s breath-hold instead of a 3 min scan time, or six slices may be acquired instead of only one in the same 3 min scan time.

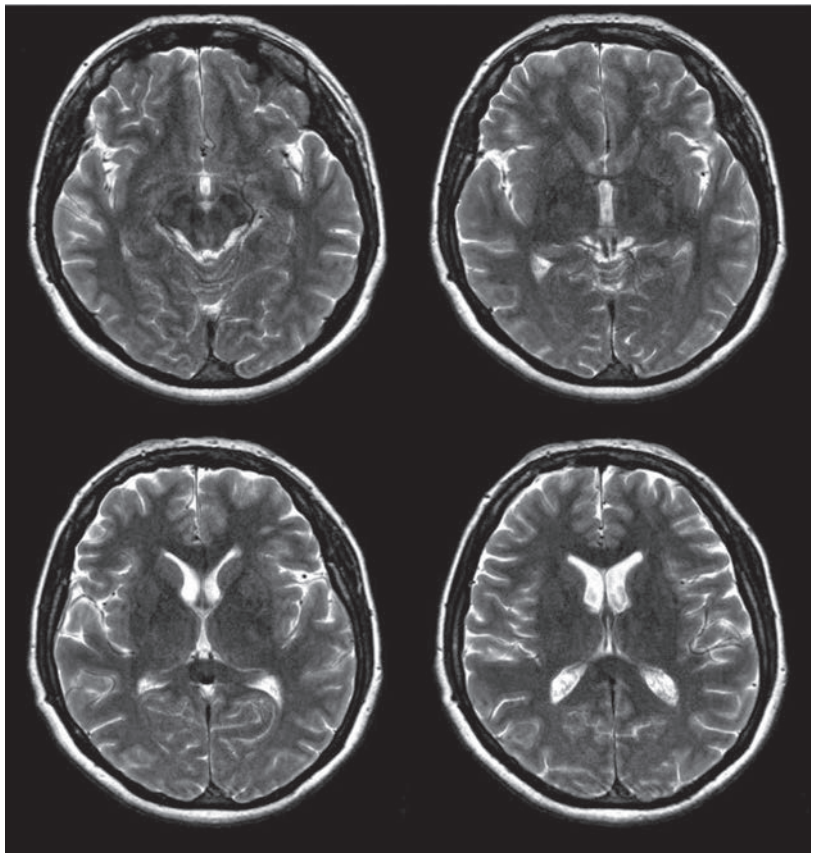

Figure 14.26 Use of parallel imaging (ASSET) to reduce acquisition time for 512 × 512 matrix acquisitions.

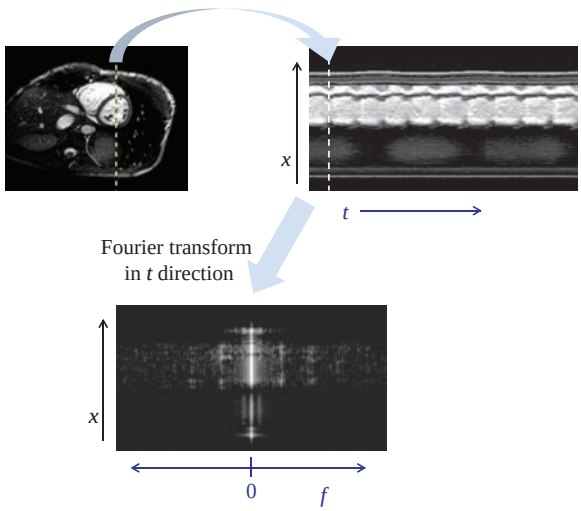

Figure 14.27 In a cine cardiac scan, most of the voxels do not change between frames. By Fourier transforming a line of pixels in the time direction, we can see the frequency distribution of voxel 'motion' (actually it is signal intensity which is changing).

In dynamic contrast enhanced imaging, the anatomy is not changing position but certain voxels will show higher intensity during the injection of gadolinium. In this situation one could acquire a training data set using a small test bolus, but it is preferable to acquire small bits of training data throughout the main bolus injection. k-t BLAST has great potential for applications in dynamic liver imaging, where we need to acquire a large number of slices at a temporal resolution of at least one frame per second.

14.8 Non-Cartesian Acquisition Schemes

Projection Reconstruction (PR) was the first MR k-space trajectory and was used by Lauterbur to produce the first MR image of two tubes of water. This method is similar to the reconstruction of

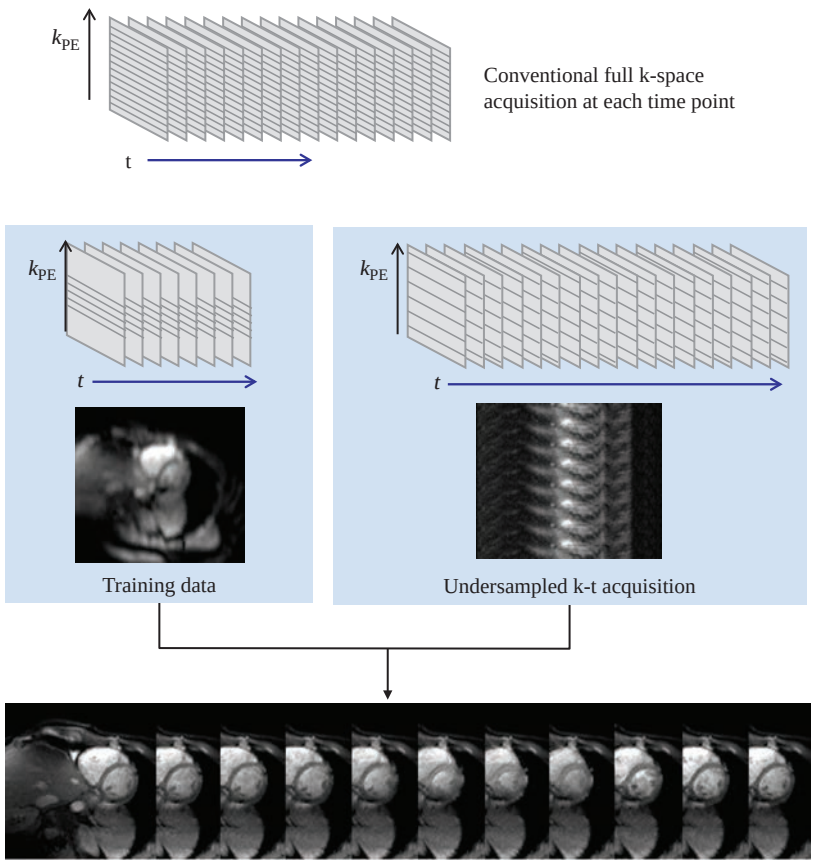

Figure 14.28 A conventional cine scan acquires the whole of k-space at every time-point. In k-t BLAST, a set of training data is acquired with low spatial and temporal resolution. This is followed by a rapid acquisition which undersamples in both k-space and time in a well-defined pattern. The training data can then be used to unwrap the aliased signals.

computerized tomography (CT) images. In CT, projections of the object are acquired at a number of angles around the object. The images are then reconstructed by 'back-projecting' the individual projections. Since simple back projection results in blurred images the projection data are usually filtered before reconstruction. In the earliest MR scanners magnetic field inhomogeneity and gradient non-linearities resulted in excessive image blurring (see Figure 1.3) and PR was subsequently replaced by the 'spin-warp' (2D FT) technique, which was much more forgiving (see Chapter 8). However with technical improvements in scanner performance PR has been reborn with a new name: radial imaging.

14.8.1 2D and 3D Radial Imaging

In radial imaging we acquire a number of projections through the object at different angles, ϕ. To produce the radial projection pattern, frequency encoding is applied simultaneously on two physical axes (e.g. x and y for transverse slices) with varying amplitudes to produce the rotational pattern. The pulse sequence simply involves slice selection and frequency encoding; there is no concept of a phase-encoding direction. Figure 14.29a shows a 2D gradient-echo radial sequence and 12 radial projections overlaid on a Cartesian k-space. In Figure 14.29b the sequence is shown for the projection at $\phi = 45°$ i.e. the G_x and G_y gradients have the same amplitude. The radial approach can also be extended into 3D by acquiring radial projections with components along x, y and z. This has sometimes been termed a Koosh ball trajectory due to its similarity with the child's toy and adult stress-buster!

In radial imaging the data are not reconstructed using filtered back projection but are 're-gridded' onto a conventional Cartesian (x,y) k-space and then reconstructed via direct Fourier transformation (see Box 'Re: Gridding').

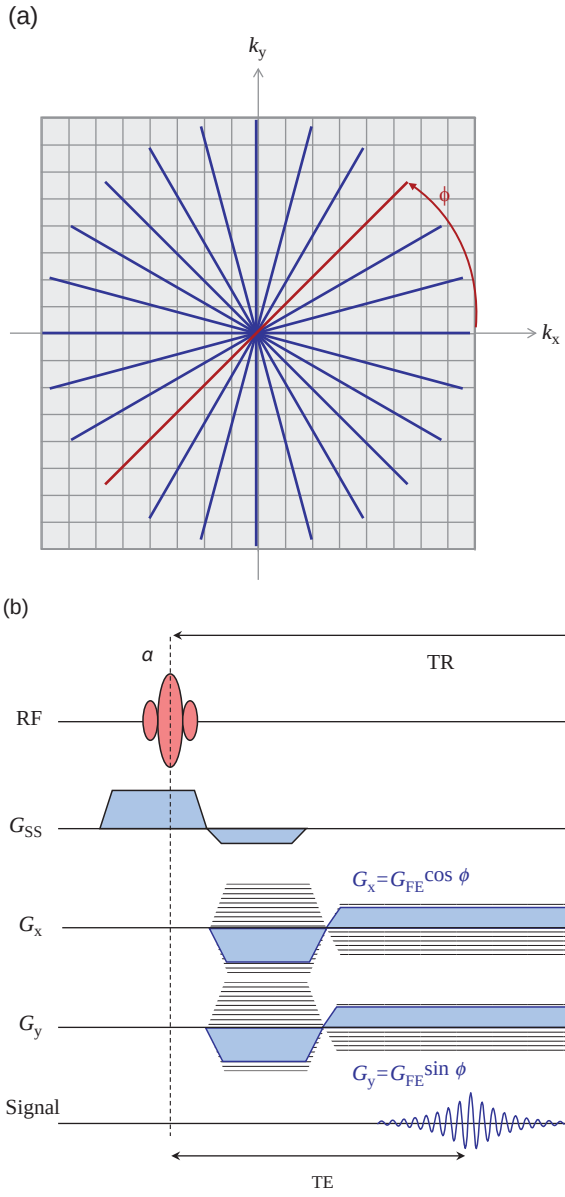

Figure 14.29 Radial scanning: (**a**) k-space for radial acquisition, the projection for $\phi = 45°$ shown in red. Re-gridding to the underlying Cartesian k-space is required prior to reconstruction. (**b**) Pulse sequence for radial acquisition for $\phi = 45°$. There is no phase encoding and the amplitude of G_x and G_y vary to produce the radii.

Re: Gridding

In conventional MRI raw data are acquired along a uniformly sampled rectilinear k-space trajectory and the image reconstructed by direct Fourier transformation. In radial and spiral imaging the k-space trajectories are non-uniform. While any non-uniform data can be reconstructed using extensions of the standard discrete Fourier transform (DFT) algorithm the methods are generally far too slow to be clinically useable. Instead, in a process called 're-gridding', the data are re-sampled or interpolated onto a uniform rectilinear grid prior to a standard FFT. Figure 14.30 shows the principle of gridding in a very simple way, where each acquired data point contributes to the signal in four nearest neighbours on the Cartesian grid. An important part of gridding is that the data also need to be corrected for the non-uniform sampling density, i.e. some sequences

like radial and spiral imaging heavily oversample the centre of k-space. Each data acquisition point therefore needs to be multiplied by an appropriate 'weighting' factor to compensate for this effect, usually based on a Bessel function.

Clinical Applications of Radial Imaging: Ultra-Short TE

Radial imaging has a number of advantages. First, because no phase-encoding gradient is used the minimum TE for gradient-echo based radial imaging can be made very short if the acquisition starts at the centre of k-space. Using non-selective or half-pulse excitation together with half-Fourier readout and ramped sampling TE can be as short as a few hundred microseconds. Furthermore, if hardware changes are made to the system such that system delays and switching times are substantially reduced then echo times as short as 8 μs can be achieved. This makes it possible to image previously unobservable tissues such as cortical bone, tendons, ligaments and menisci, which have very short T_2 (Figure 14.31). The term ultra-short TE is used to describe these applications and it gives us another new acronym, UTE. The UTE images themselves are heavily PD-weighted, so it is common to acquire a second echo at a later time (e.g. 4 ms) and subtract it from the UTE image. The subtracted image highlights the short T_2 tissues as bright structures against a darker background.

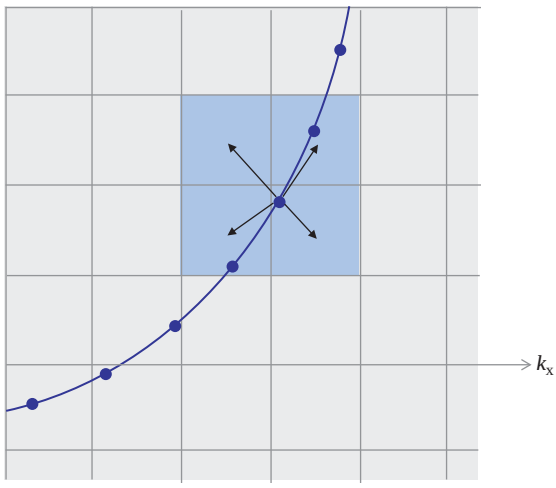

Figure 14.30 Re-gridding: each point affects the four nearest neighbours. The blue line and points represent actual k-space trajectory and sampled points.

Stealth Mode: Silent Scanning

The use of a 2D or 3D centre-out k-space trajectory means that the gradient amplitudes only need to change very slightly between TRs. Since the majority of the acoustic noise is associated with gradient switching this makes the sequences considerably quieter. Figure 14.32 shows the *x* and *y* gradient waveforms for a simulated 2D radial sequence with 36 spokes. The reduced amplitude of the gradient transitions between TRs can be clearly seen. Of course in this case we have ignored the conventional slice-selection gradient which would still create noise. Implementing this sequence as a 3D volume acquisition with very short, non-selective RF pulses can produce an almost totally silent acquisition, and the magnet cold head then becomes the noisiest component in the magnet room. While there are many advantages to silent scanning, particularly for babies, it is a weird experience for those of us who are scanned regularly and like to count the gradient pulses!

Sampling in Radial Imaging

The oversampling of the centre of k-space means that radial acquisitions take $\pi/2$ times longer than conventional Cartesian acquisitions for the same matrix. The scan time can be reduced by undersampling the radial data, i.e. decreasing the number of spokes. In conventional Cartesian imaging this results in image aliasing. In radial imaging it results in radially positioned streak artefacts (Figure 14.33). In the same way as for undersampled Cartesian imaging, reducing the number of radial spokes does not compromise spatial resolution but reduces SNR and leads to increased streaking artefacts. However, with a high enough degree of undersampling the artefacts become a nearly uniform background haze instead of discrete streaks. With an appropriate trade-off between acquisition time and artefact, undersampled PR offers a means of rapidly acquiring high-resolution images.

14.8.2 Spiral

In spiral imaging the k-space trajectory samples data along an Archimedean spiral (see Box 'k-Space Spirograph'). Spiral acquisitions can achieve greater scan efficiency than conventional Cartesian acquisitions, i.e. a spiral acquisition can cover a greater portion of k-space with each RF excitation. As the spiral readout starts at the centre of k-space, spiral sequences can have very short echo times. Spiral acquisitions may be

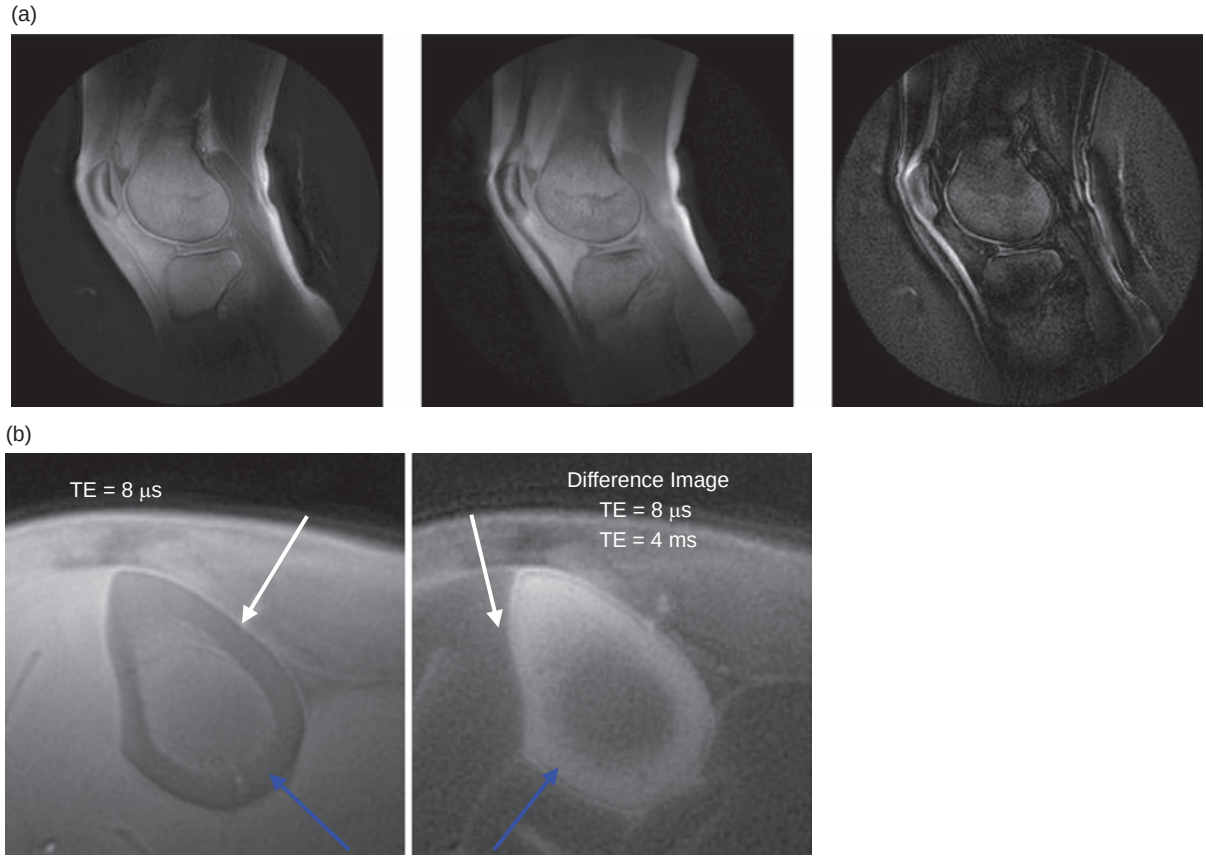

Figure 14.31 (**a**) Ultra-short TE images of normal knee: FID, gradient echo and subtracted image which highlights the short T_2 components such as the femoro-patellar tendon. Images courtesy of Philips Healthcare. (**b**) Normal tibia: FID and subtracted image, showing high signal in cortical bone (T_2 = 500 μs, blue arrows) and periosteum (T_2 = 5–11 ms, white arrows). Images courtesy of Jean Brittain, GE Healthcare.

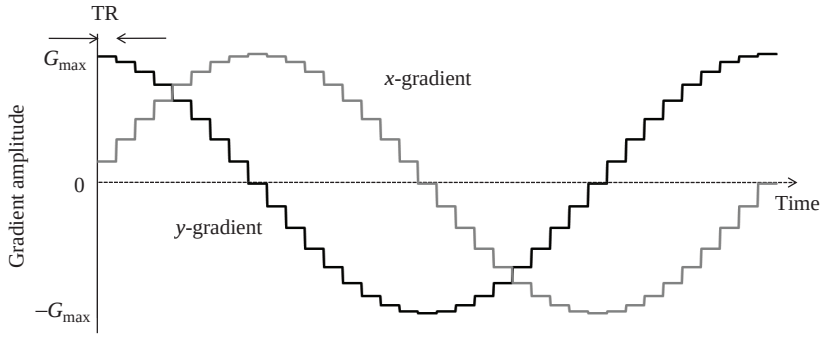

Figure 14.32 In-plane (*x* and *y*) gradient activity for a simulated 2D centre-out radial acquisition. Note the reduced amplitude transitions, i.e. switching, between TRs. The reduced gradient switching results in a considerable reduction in acoustic noise.

either single-shot or multi-shot. In a single-shot acquisition all of the k-space data are acquired following a single RF excitation. Figure 14.34 shows the k-space trajectory for a single-shot acquisition and the in-plane gradient waveforms required to generate this trajectory. Like radial imaging, there is no longer any concept of phase or frequency encoding and data are constantly acquired during the spiral readout.

For multi-shot acquisitions, a number (N_{shot}) of spiral interleaves are performed, each shot being

rotated by an angle of $\pm 2\pi/N_{shot}$ (Figure 14.35). Figure 14.36 shows a phantom image acquired with a single-shot spiral comprising 16 384 complex data points, and a multi-shot acquisition with 16 interleaves each of 4096 data points.

Since spirals are a method of in-plane data readout then they can be combined with any other pulse sequences, for example spin echo. The spirals can also be acquired in a reverse fashion so that the centre of k-space is acquired last. This is one way of acquiring a T_2^*-weighted spiral acquisition suitable for fMRI studies. Spirals can also be extended to 3D, the simplest method being to incorporate a conventional slice-select phase encoding; the resultant data are often called a stack of spirals.

Figure 14.33 Radial artefacts: streak artefacts (very similar to CT) can be seen in the background.

k-Space Spirograph

Spiral trajectories use an Archimedean spiral which is defined by

$$r = a\theta$$

where r is the radius, a is a constant and θ the angle. The k-space path for a simple constant spacing spiral is given by

$$k_x = \frac{N_{shot}}{2\pi \cdot FOV}\theta \sin\theta$$

$$k_y = \frac{N_{shot}}{2\pi \cdot FOV}\theta \cos\theta$$

where N_{shot} is the number of interleaved spirals or shots. The gradient waveforms necessary to produce a spiral k-space trajectory come from the derivative of k with respect to time:

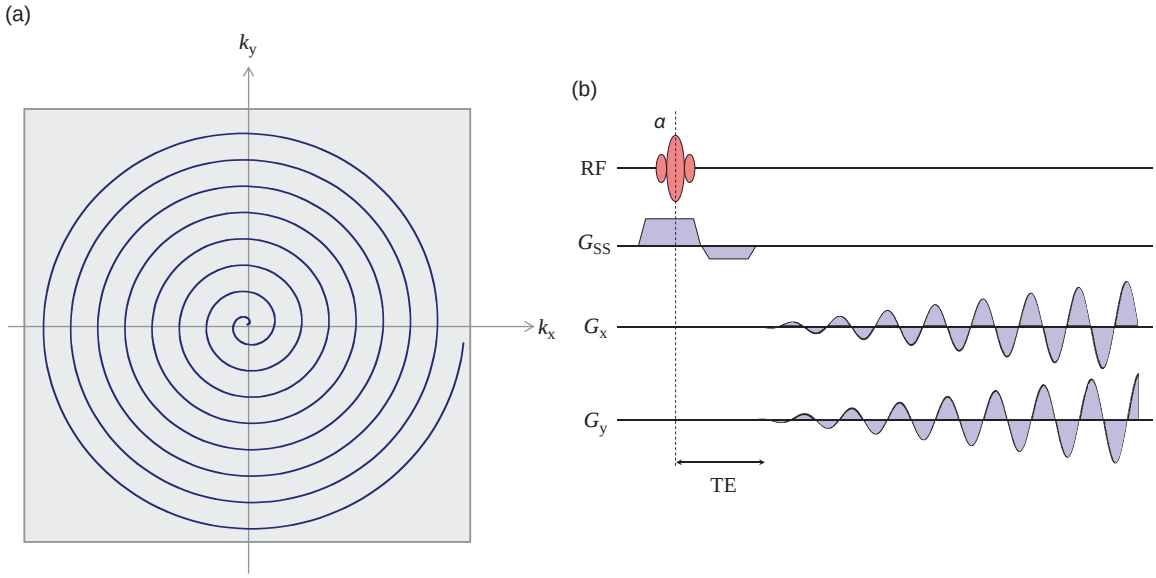

Figure 14.34 (a) k-space for single-shot spiral acquisition, (b) spiral pulse sequence to generate the k-space trajectory in (a).

$$G_x = \frac{N_{shot}}{\gamma \cdot FOV}\frac{d\theta}{dt}(\sin\theta + \theta\cos\theta)$$

$$G_y = \frac{N_{shot}}{\gamma \cdot FOV}\frac{d\theta}{dt}(\cos\theta - \theta\sin\theta)$$

These are shown in Figure 14.34a. In practice, slew rate constraints need to be considered and the rotation velocity $d\theta/dt$ may not be constant.

Problems with Spirals

The major problem with spiral acquisitions is the blurring due to off-resonant spins. These frequency offsets can come from B_0 field inhomogeneity, local susceptibility effects and chemical shifts. In conventional Cartesian imaging these frequency offsets result in a simple shift in the frequency-encoding direction – e.g. chemical shift artefact – while in spiral imaging, since the trajectory is changing simultaneously in both in-plane directions the effect is a 2D blurring (Figure 14.36c). To reduce this blurring spiral imaging sequences are usually performed with a water-only excitation (spatial-spectral) (Chapter 12). To correct for the effects due to B_0 inhomogeneity, it is usual for the system to rapidly acquire a field map to determine the frequency offset as a function of spatial location. This can easily be done during the prescan period by acquiring two single-shot spiral images with slightly different TEs and constructing a phase map by complex subtraction. The calculated frequency shifts can then be incorporated into the spiral gridding algorithm to correct for the off-resonance spins.

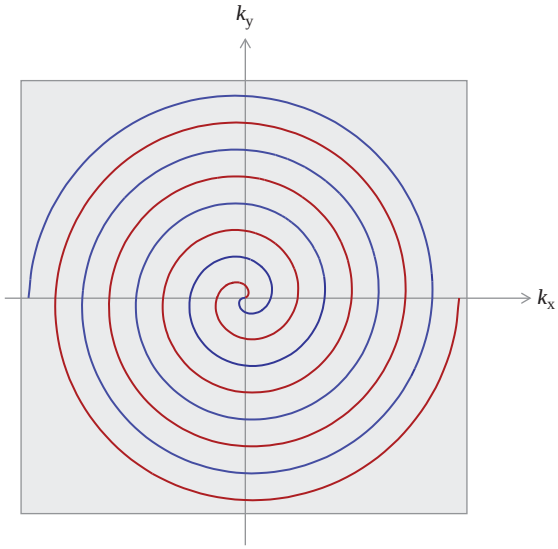

Figure 14.35 Multi-shot spiral k-space with two interleaved shots.

14.9 Compressed Sensing

Compressed Sensing (CS) is a new method of accelerating image acquisition that is based upon the concepts used in image compression. We are all familiar with the concept of compressing images or movies to reduce the space required for storage. The Joint Photographic Experts Group (JPEG) standard is a typical example of a compressed image format that is extensively used to reduce the size of image files, while the Motion Picture Encoding Group (MPEG) standard is used to compress video. Both can be performed with little or no reduction in image information. JPEG, for example, exploits redundancies in the data and can typically achieve 10:1 compression without any perceptible loss of image quality.

CS essentially involves this process in reverse. We sample a reduced number of data points and then iteratively reconstruct the image by estimating the missing data points. There are, however, a number of requirements for CS to work in the context of MRI.

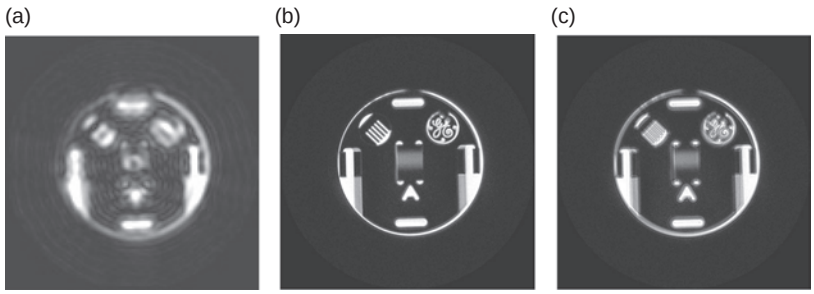

Figure 14.36 (**a**) Single-shot spiral image; (**b**) 16-shot interleaved spiral image; (**c**) 16-shot interleaved spiral but with 50 Hz offset.

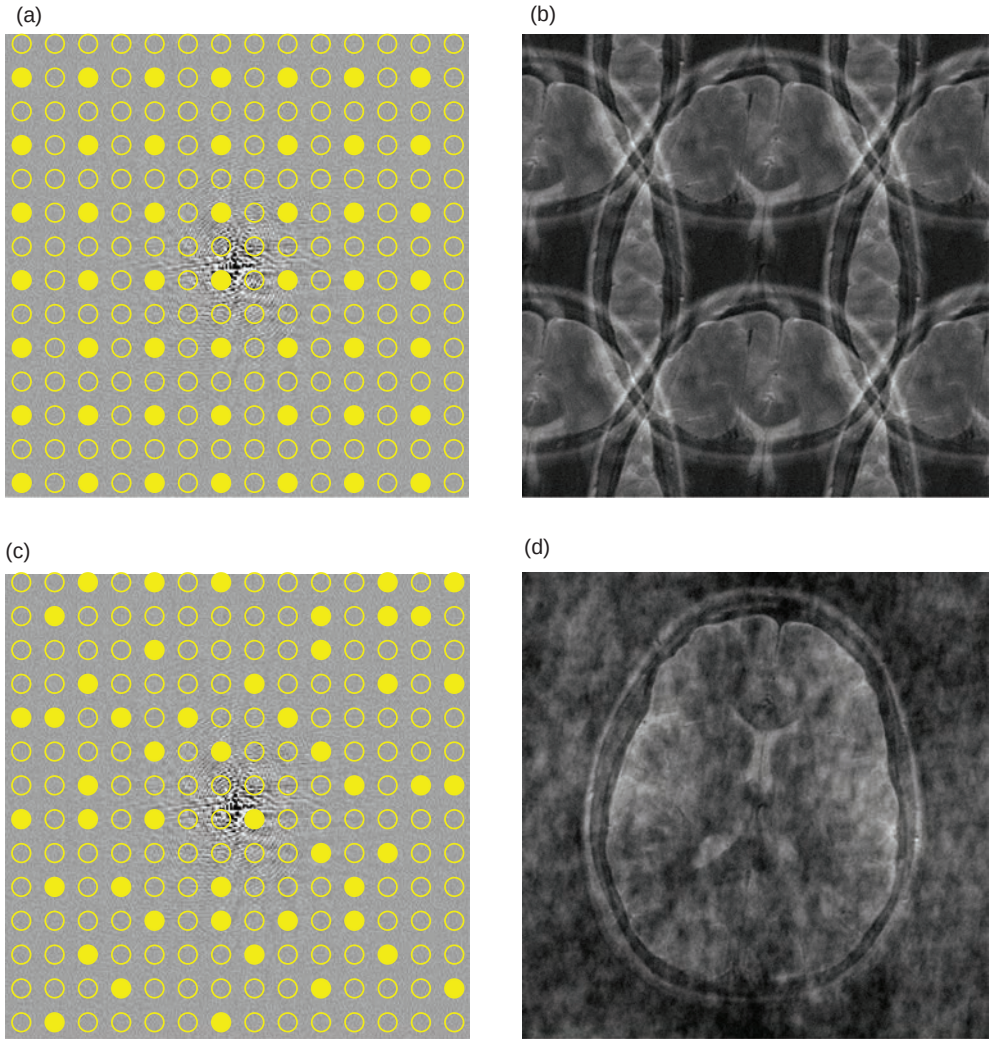

Figure 14.37 Principles of compressed sensing. (**a**) Regularly undersampled (25% of the original data), k-space. (**b**) The image obtained following standard 2D Fourier transformation – note the coherent image aliasing. (**c**) A random 2D undersampling pattern (33% of the original data. (**d**) The image reconstructed using a standard Fourier transform – note the incoherent artefacts now appear as an increase in background 'noise'.

First, the data must be sparse, or be transformed into a sparse representation. Sparsity in this context means that the data contain very little information. An MR angiogram is a good example of sparse data in the image domain. There are only a few voxels containing signal of interest, while the rest of the image is essentially blank. Other images may require some form of transformation to make them sparse – for example, the voxels in a standard brain image are relatively smooth-changing with location, i.e., two adjacent voxels are likely to be very similar. Therefore a suitable sparsifying transform could be to simply take the difference between adjacent voxels. In practice more sophisticated sparsifying transformations are used, such as the discrete cosine transformation (DCT) used in JPEG compression or the wavelet transformation used in JPEG-2000 compression. In a dynamic MRI acquisition there is very little change between adjacent temporal frames, so temporal differences can also be used to sparsify dynamic data. Second, the aliasing artefacts caused by the sub-sampling of k-space must be incoherent (noise-like). We know that regular sub-sampling of k-space results in foldover artefacts (Figure 14.37a,b).

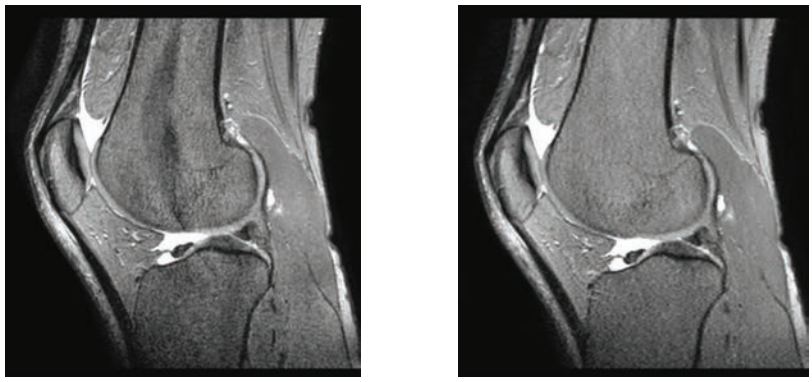

Figure 14.38 Image of the knee using (**a**) conventional parallel imaging (SENSE) with reduction factor of 4; (**b**) compressed sensing with undersampling factor of 4.

These are coherent artefacts, whereas if we randomly sample k_y space then the resulting incoherent artefacts appear much more like background 'noise' (Figure 14.37c,d).

The quality of a CS reconstruction is very dependent upon the sparse sampling pattern. As we already know, the bulk of the contrast in an image is at the centre of k-space, so a CS sampling pattern usually fully samples the centre of k-space and then more randomly samples the periphery.

CS reconstructions are best used with 3D acquisitions where it is relatively straightforward to subsample in k_y–k_z space. Since 3D imaging is inherently time-consuming, any acceleration technique can have a significant impact on overall acquisition times. Non-Cartesian sampling schemes, such as radial or spiral, are also attractive from a CS perspective since undersampling artefacts are incoherent. CS can be combined with parallel imaging, but the requirement for random sampling required by CS conflicts with the requirement for large sampling gaps, therefore careful choices need to be made in terms of the random sampling distribution. Figure 14.38 shows how the randomized undersampling schemes used in CS produce fewer artefacts than conventional regularly undersampled acquisitions.

See also:

- Totally fazed: phase encoding: Section 8.5.2
- Phased array coils: Section 10.5.2

Further Reading

Bernstein MA, King KF and Zhou XJ (2004) *Handbook of MRI Pulse Sequences*. London: Elsevier Academic Press, chapters 13 and 17.

Brown RW, Cheng YCN, Haacke EM, Thompson MR and Venkatesan R (2014) *Magnetic Resonance Imaging: Physical Principles and Sequence Design*, 2nd edn. Hoboken, NJ: John Wiley & Sons, chapters 14 and 19.

Griswold MA, Jakob PM, Heidemann RM, *et al.* (2002) 'Generalised autocalibrating partially parallel acqusitions (GRAPPA)'. *Magn Reson Med* 47:1202–1210.

Lustig M, Donoho D and Pauly JM (2007) 'Sparse MRI: the application of compressed sensing for rapid MR imaging'. *Magn Reson Med* 58:1182–1195.

Pruessmann KP, Weiger M, Scheidegger MB and Boesiger P (1999) 'SENSE: sensitivity encoding for fast MRI'. *Magn Reson Med* 42:952–962.

Sodickson DK and Manning WJ (1997) 'Simultaneous acquisition of spatial harmonics (SMASH): fast imaging with radiofrequency coil arrays'. *Magn Reson Med* 38:591–603.

Tsao J, Boesiger P and Pruessman KP (2003) 'k-t BLAST and k-t SENSE: dynamic MRI with high frame rate exploiting spatiotemporal correlations'. *Magn Reson Med* 50:1031–1042.